

STRUCTURE AND SUBHALO POPULATION OF HALOS IN A SELF-INTERACTING DARK MATTER COSMOLOGY

PEDRO COLÍN AND VLADIMIR AVILA-REESE,

Instituto de Astronomía, Universidad Nacional Autónoma de México, A.P. 70-264, 04510, México, D.F.,

México

OCTAVIO VALENZUELA

Astronomy Department, New Mexico State University, Box 30001, Department 4500, Las Cruces, NM

88003-0001

AND

CLAUDIO FIRMANI

Osservatorio Astronomico di Brera, via E. Bianchi 46, 23807 Merate (LC), Italy

Subject headings: cosmology:dark matter — galaxies:formation — galaxies:halos — methods:N-body simulations

accepted by the *Astrophysical Journal*

ABSTRACT

A series of high-resolution numerical simulations were performed to study the structure and substructure of Milky Way (MW)- and cluster-sized halos in a Λ -Cold Dark Matter (CDM) cosmology with self-interacting (SI) dark particles. The cross section per unit of particle mass has the form $\sigma_{DM} = \sigma_0(1/v_{100})^\alpha$, where σ_0 is a constant in units of $\text{cm}^2\text{gr}^{-1}$ and v_{100} is the relative velocity in units of 100 km s^{-1} . Different values for σ_0 with $\alpha = 0$ or 1 were used. For small values of $\sigma_{DM} = \text{const.}$ ($\lesssim 0.5$, $\alpha = 0$), the core density of the halos at $z = 0$ is typically higher at a given mass for lower values of σ_0 or, at a given σ_0 , for lower masses. For values of σ_0 as high as 3.0 , both cluster- and MW-sized halos may undergo the gravothermal catastrophe before $z = 0$. The core expansion occurs in a stable regime because the heat capacity, C , is positive in the center. After the maximum expansion, the isothermal core is hotter than the periphery and $C < 0$. Then, the gravothermal catastrophe triggers. The instability onset can be delayed by both the dynamical heating of the halo by major mergers and the interaction of cool particles with the hot environment of a host halo. When $\alpha = 1$, the core density of cluster- and MW-sized halos is similar. Using $\sigma_{DM} = 0.5 - 1.0 (1/v_{100})$, our predictions agree with the central densities and the core scaling laws of halos both inferred from the observations of dwarf and low surface brightness galaxies and clusters of galaxies. Regarding the cumulative v_{max} -function of subhalos within MW-sized halos, when $(\sigma_0, \alpha) = (0.1, 0.0)$, $(0.5, 0.0)$ or $(0.5, 1.0)$ it agrees roughly with observations (luminous satellites) for $v_{\text{max}} \gtrsim 30 \text{ km s}^{-1}$, while at $v_{\text{max}} = 20 \text{ km s}^{-1}$ the functions are already a factor 5-8 higher, similar to the CDM predictions. For $(\sigma_0, \alpha) = (1.0, 1.0)$, this function lies above the corresponding CDM function. The structure and number of subhalos are affected by the scattering properties of the host halo rather than by those of the subhalos. The halos with SI have more specific angular momentum at a given mass shell and are rounder than their CDM counterparts. However, the angular momentum excess w.r.t. CDM is small. We conclude that the introduction of SI particles with $\sigma_{DM} \propto 1/v_{100}$ may remedy the cuspy core problem of the CDM cosmogony, at the same time keeping a subhalo population similar to that of the CDM halos.

1. INTRODUCTION

The current paradigm for cosmic structure formation is based on the cold dark matter (CDM) cosmological models, where CDM particles are assumed to be collisionless. This is the simplest assumption about the nature of these particles, not yet detected. The predictions of the most popular incarnation of the CDM variants, the spatially flat with a non-vanishing cosmological constant model, are in excellent agreement with a large body of observational data at large scales. With the advent of high-resolution numerical simulations and new observational techniques, a comparison between models and observations at small scales has become possible. Apparent conflicts have emerged as a result of this comparison: (i) the predicted halo inner density profiles are cuspy, in disagreement with the shallow cores favored by observations of dwarf and low surface brightness galaxies (LSB), and (ii)

the predicted number of subhalos within Milky Way-sized (MW-sized) halos overwhelm the observed abundance of satellite galaxies in the Local Group.

Recently, a plethora of alternative theories, which modify the predictions of the CDM model at small scales but retain its successes at large scales, have been proposed (e.g., Davé et al. 2001 and references there included). In one of these scenarios, CDM particles are assumed to be self-interacting (SI) in such a way that the heat flux to the core smooths out the density cusp, and simultaneously reduces the amount of substructure by evaporating orbiting subhalos (Spergel & Steinhardt 2000). Several authors have explored this model numerically and analytically and concluded that the relevant regime for structure formation would have to be the optically thin one (Moore et al. 2000; Yoshida et al. 2000a; Firmani et al. 2001b; Kochanek & White 2000; Davé et al. 2001; Hennawi &

Ostriker 2001; Balberg, Shapiro, & Inagaki 2002). By means of cosmological N-body simulations, using a *constant* cross section per unit mass, σ_{DM} , Davé et al. (2001) found that halos at galaxy scales have long-lived shallow cores whose sizes agree with observational inferences when $\sigma_{DM} \approx 5 \text{ cm}^2\text{gr}^{-1}$. At the cluster scales, Yoshida et al. (2000b) also found that the SIDM halos present long-lived shallow cores. According to them, σ_{DM} should be smaller than $\approx 5 \text{ cm}^2\text{gr}^{-1}$ in order for their results to be in agreement with observations of cluster of galaxies.

On the other hand, N-body simulations of relaxed, isolated, SI dark matter (SIDM) halos with initial cuspy density profiles and with a relatively high σ_{DM} value show a core evolution which is remarkably rapid. After the maximum soft core radius is reached, in time scales of the order of the halo dynamical time, the core collapse is triggered almost immediately (Kochanek & White 2000, hereafter KW; Burkert 2000; see also Quinlan 1996). Davé et al. (2001) argue that the fast core collapse seen in these simulations may be attributed to the absence, in the isolated case, of infalling dynamically-hot material. Davé et al. also find that the central density of simulated cosmological halos (at $1 \text{ h}^{-1}\text{kpc}$ from the center) remains approximately constant with halo mass, a result actually not expected for a constant σ_{DM} (Yoshida et al. 2000b; Firmani et al. 2001a,b). In fact, Firmani et al. (2001b) find that ρ_c is nearly independent of halo mass only when σ_{DM} is *inversely proportional to the relative velocity of colliding particles*. They used a numerical code based on the collisional Boltzman equation and took into account the cosmological mass aggregation process during the formation of their spherical symmetric halos. They obtain a central density of $\rho_c \approx 0.02 M_\odot \text{pc}^{-3}$ (a value inferred from observations, $h = 0.65$ was assumed, Firmani et al. 2000a) for $\sigma_{DM} \approx (0.6/v_{100}) \text{ cm}^2\text{gr}^{-1}$, where v_{100} is the relative velocity v_{12} in units of 100 kms^{-1} .

As suggested by all these studies, important questions regarding the SIDM cosmology still remain without a satisfactory answer or without an answer at all. Do the SIDM cosmological halos undergo a core collapse on scales times shorter than a Hubble time? How does the cosmological mass aggregation history (MAH) affect the core evolution? Does a constant cross section produce halos with a nearly constant central density regardless of their mass? Which are the predictions for SIDM models with a cross section inversely proportional to v_{12} ? How is the subhalo population at cluster and galaxy scales in a SIDM cosmology? In this paper, we will address these questions using high-resolution cosmological simulations of cluster- and galaxy-sized halos with $\sigma_{DM} \propto \text{const}$ and $\propto 1/v_{12}$.

Our study is aimed to explore whether the SIDM model predictions are in better agreement with observations than the CDM ones. As already discussed above, the key parameter for SIDM is the interaction cross section,

$$\sigma_{DM} = \sigma_0 \left(\frac{1}{v_{12}} \right)^\alpha. \quad (1)$$

A number of authors have attempted to constrain the range of values for the pair of parameters (σ_0, α) (Firmani et al. 2000, 2001a; Miralda-Escudé 2000; Wandelt et al. 2000; Meneghetti et al. 2001; Gnedin & Ostriker

2001; Hennawi & Ostriker 2001). According to analytical and semi-analytical arguments of Hennawi & Ostriker (2001; HO hereafter), σ_{DM} should be large enough to produce a shallow core in agreement with observations, but small enough so the core halo would not collapse in a Hubble time or subhalo evaporation within cluster-sized halos would not alter dramatically the elliptical Fundamental Plane relations. This leaves the SIDM cosmology with a limited range of (σ_0, α) values. HO also introduce an extra strong constrain for SIDM, the mass of a central black hole in the MW and the lack of it in M33. According to them, accretion of SIDM onto seed black holes produces holes that can be much more massive than those observed if σ_{DM} is roughly as large as needed to form the soft cores inferred from observations. In §5.2 we will discuss this constrain in light of our results.

In §2 we describe the method and strategy to simulate SIDM halos, and present the simulation of a monolithic halo (§2.1) as well as the cosmological simulations carried out in this paper (§2.2). In §3.1 we analyze the density profiles and central densities measured in our simulated cluster- and galaxy-sized halos with different values of (σ_0, α) and different merging histories. In §3.2 we discuss the concentration parameters of halos and subhalos, while in §3.3 and 3.4 we present results regarding the ellipticity and angular momentum distribution of the SIDM halos. Section 4 is devoted to the study of the subhalo population in the MW- and cluster-sized SIDM halos. In §5 we discuss our results and the viability of the SIDM models, and in §6 we summarize this paper and present our conclusions.

2. SIMULATIONS

The Adaptive Refinement Tree (ART) N-body code (Kravtsov, Klypin, & Khokhlov 1997) has been used to run the N-body simulations. The ART code achieves high spatial resolution by refining the base uniform grid in all high-density regions with an automated refinement algorithm. The elastic collisions, characterized by a scattering cross section σ_{DM} , are implemented in ART in the following manner. In a medium with density ρ , the predicted distance d that a particle travels without collisioning is given by (Gibbs 1994)

$$d = -\lambda \ln(1 - P), \quad (2)$$

where $\lambda = 1/\rho\sigma_{DM}$ is the mean free path and P is a random number distributed uniformly between 0 and 1. A pair of particles collide if this distance d results lower than the distance $v_{12}\Delta t$, where v_{12} is the relative velocity between the particle and *one of* its nearest neighbors, and Δt is the time step. In an inhomogenous medium, we substitute ρ by the local density at the particle's position, ρ_i . We exploit the mesh hierarchy structure of ART to evaluate both the local density and the relative velocity. On each level of the structure, starting from the finest level, ART assigns the density in each *cell* using the standard cloud-in-cell technique (Hockney & Eastwood 1981). The density at the particle's position is found by interpolation¹ using cloud-in-cell. The search for a partner to collide with may involve many neighbor cells

¹In ART, only those cells that are not refined are allowed to own particles

and more than one level. We find that the search for partners of particles that lie in low-density regions fails often; this, however, does not affect our results because collisions in these regions are very rare. It happens many times that the partner is found in the same cell where the particle is, and thus the search is limited to only one cell. The new velocities after collision are computed by imposing energy and momentum conservation and by orienting the after-collision relative velocity randomly.

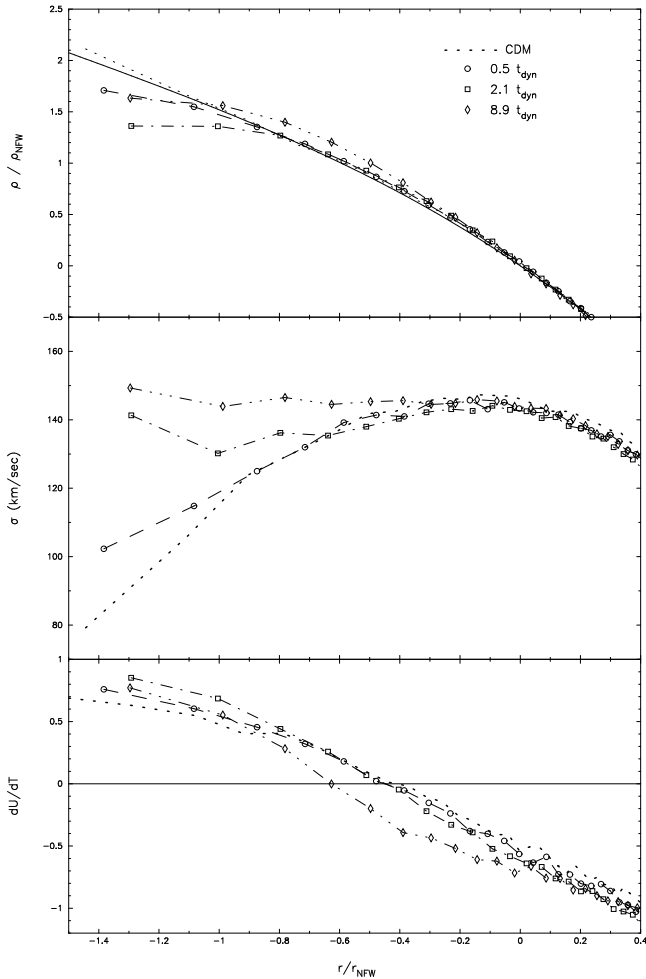


FIG. 1.— Evolution of the density, 3D velocity dispersion, and heat capacity profiles (top, central and bottom panels, respectively) for the NFW isolated SIDM halo of mass $2 \times 10^{11} h^{-1} M_{\odot}$ and initial concentration $c_{\text{NFW}} = 14$. The maximum expansion of the core occurs at about $2t_{\text{dyn}}$. With a solid line is represented the analytical NFW function from which a relaxed and stable dark matter halo is reproduced (dotted line). We see that at $9 t_{\text{dyn}}$ the central density has increased by almost a factor 2.

2.1. Self-Interacting simulations of a monolithic halo

In order to test our collisional algorithm on ART code we ran a simulation of a monolithic (isolated) halo of 3×10^5 particles with an initial NFW density profile, and SI turned on. The virial mass of the halo is $M_{\text{vir}} = 2 \times 10^{11} h^{-1} M_{\odot}$, with a NFW concentration of $c_{\text{NFW}} = 14$.

If we assume the Hernquist model to have the same density as the NFW one in the central r^{-1} region, we can relate the scale radius r_H of the Hernquist density profile with c_{NFW} . Given r_H and σ_{DM} we can estimate the dimensionless cross section $\hat{\sigma}$ and the core relaxation time t_{rc} , both as defined by Kochanek & White (2000, hereafter KW) who also simulated SIDM monolithic halos but with a Hernquist profile. The simulation was run when the SI algorithm was still on test and used the particle velocity for the computation of the collisional probability instead of v_{12} ; this produces a smaller scattering rate than when one uses v_{12} (KW). The model has $\sigma_{DM} = 9.0 \text{ cm}^2 \text{ gr}^{-1}$.

The evolution of the density, 3D velocity dispersion, and heat capacity profiles are shown in Figure 1; time is measured in units of the dynamical time, t_{dyn} , as defined in KW. The evolution proceeds in much the same way as in previous similar SI simulations (e.g., Burkert 2000; KW). If the initial equilibrium configuration of a halo has a NFW density profile, the velocity dispersion (temperature) profile peaks out of the center, close to the scale radius r_{NFW} (dotted line in Fig. 1); i.e., there is an inversion of the temperature profile. We have measured the potential, kinetic, and total energy, W , T , and U , respectively, of our monolithic halo as a function of radius and found, for the initial configuration, that both the total energy (see also Fig. 2 of Lokas & Mamon 2001) and the heat capacity, C , of the innermost region are positive (see Fig. 1).

Therefore, when the SI is turned on, heat starts flowing into the core from the immediate surroundings and the core expands. An increase in the core's total energy produces an increase in the core's temperature and in the ratio $2T/|W|$; in fact, the maximum expansion of the core occurs approximately when $2T/|W|$ also reaches its maximum. At this point the core is isothermal and the temperature inversion is gone (Fig. 1; see also panel (a) in Fig. 2). Now, the isothermal core is hotter than the surroundings and heat starts flowing outwards (note that this process happens in the outer central region where C is already negative). The central region, where both U and C are positive, reduces in size (Fig. 1). The core loses heat and contracts; the system is unstable and the gravothermal catastrophe phase triggers (see Binney & Tremaine 1987, §8.2): the core becomes hotter as it loses energy outwards, and the increased temperature difference leads to an even faster energy loss with the consequent core shrinking (panel (b) in Fig. 2).

An interesting question is whether the inverse instability, the gravothermal expansion, may arise sometime in the evolution of a halo. This brings us to the question: why at the beginning of the SI evolution of the isolated halo, when there is an inversion of the temperature profile, a run-away core expansion does not occur? The reason is that the central region has positive total energy and heat capacity. Let us now analyze the halo after the maximum core expansion and let us assume that for some reason (for example, kinetic energy injection by mergers), the outer region of a halo becomes hotter than the isothermal core (panel (c) in Fig. 2). The system in this case does not obey the conditions for the gravothermal expansion instability because, again, U and C in the central region are positive (due to the strong halo heating, C may become positive even at the periphery). A flow of heat into the core makes it expand and brings most parts of the system

to an isothermal state (panel (c)), which might be unstable to core collapse because the isothermal sphere becomes a local entropy minimum rather than a local entropy maximum. Thus, the core collapse phase for cosmological SIDM halos can be delayed due to an external energy injection, *but not reversed*. We will return to this discussion in §3 where we analyze cosmological SIDM halos.

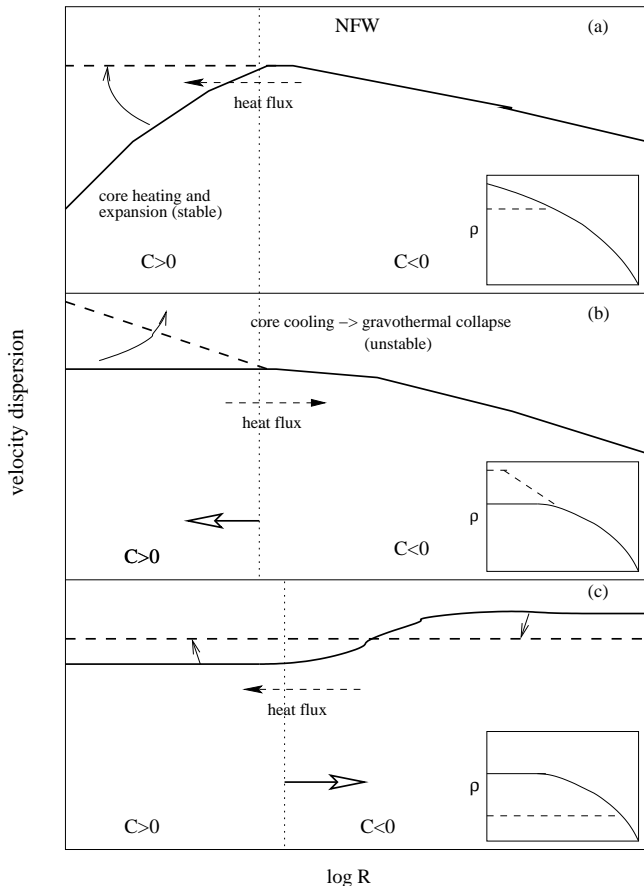


FIG. 2.— Schematical behavior of the 3D velocity dispersion (temperature) profile in a SIDM halo, and of the logarithmic density profile (encapsulated boxes). Panels (a), (b), and (c) show the core expansion phase (stable), the gravothermal catastrophe phase (unstable), and the core collapse delay (and core expansion) when the halo is externally heated, respectively. See the text for more explanations. C is the heat capacity.

The notion of gravothermal catastrophe has been introduced for a non-singular isothermal model (Lynden-Bell & Wood 1968). Although in the cosmological case the halos are not described by isothermal spheres, the core expansion phase leads a significant part of the SIDM halo to a state close to that of a non-singular sphere. This is for example the case of the halo at maximum expansion in Fig. 1 (squares) where $r_c \approx (9\sigma^2/4\pi G\rho_c)^{1/2}$ and r_c is roughly equal to the radius where C is still positive. Interestingly, the state of this halo is close to the non-equilibrium state of minimum entropy described by Lynden-Bell & Wood (1968). At the radius where the velocity dispersion (temperature) is still roughly constant

(the radius of the isothermal sphere), the density has decreased from the center by approximately a factor of 30 and E and C are already negative. Systems like this are susceptible to the gravothermal catastrophe and this is what we observe it happens in our simulations.

For our monolithic NFW halo, the maximum constant density core radius is reached approximately in 2.6×10^9 yr. This time scale agrees with the estimated core relaxation time, t_{rc} , by KW for $\hat{\sigma} \sim 0.8$ in their dimensionless units or, equivalently, $\sigma_{DM} \sim 5.0 \text{ cm}^2 \text{ gr}^{-1}$. As mentioned above, had we used v_{12} instead of the particle velocity, a higher scattering rate would have been expected. The factor 9/5, however, is lower than the factor 3 that KW claim they measure. The difference is probably due to the way in which we compute local density. If we estimate the core radius r_c by the point where the density drops to 1/4 the central density, then $r_c \sim 0.4r_{\text{NFW}}$. Using the same definition for r_c , finds $r_c \sim 0.6r_p$, where r_p is the radius where the velocity dispersion peaks for a Hernquist density profile. Because the radius r_p is close to r_{NFW} for a NFW density profile, we would have expected, for pure analogy with Burkert’s results, that $r_c \sim 0.6r_{\text{NFW}}$. We see from Figure 1, panel (b), that the peak is broad and is slightly lower than r_{NFW} . It is not thus difficult to see why the core size is not as large as in the Hernquist’s case. We let the simulation run for another 8.5×10^9 yr and compared the rate at which the core collapse is produced with that predicted by KW (see their Fig. 2). In the KW halo, for which $t_{rc} \sim 2.6 \times 10^9$ yr and $\hat{\sigma} \sim 0.8$, the core collapse develops at a faster rate than the one we observe in our halo. Our core density evolution is more akin to a KW $\hat{\sigma}$ simulation with a value between 1.0 and 3.0. It is not clear what this difference is due to, but this difference could also be explained by the fact that we are using a NFW density profile instead of a Hernquist one. In any case, we find a good agreement between our results and Burkert’s and KW results.

2.2. Cosmological simulations of SIDM halos

The set of simulations performed to analyze the structure of halos in a SIDM cosmology uses the multiple-mass variant of ART (Klypin et al. 2001) in order to increase the mass and spatial resolution in few selected halos. All models assume a Λ CDM power spectrum with total matter density and cosmological constant, in units of the critical density, of $\Omega_m = 0.3$ and $\Omega_\Lambda = 0.7$, a Hubble constant of $h = 0.7$, in units of $100 \text{ km s}^{-1} \text{ Mpc}^{-1}$, and a $\sigma_8 = 1.0$. Here σ_8 represents the rms of mass fluctuations estimated with the t op-hat window of radius $8h^{-1} \text{ Mpc}$.

We first perform two low-mass resolution simulations, one in a $100 h^{-1} \text{ Mpc}$ box and the other in a $12.5 h^{-1} \text{ Mpc}$ box. Both simulations were run with 64^3 particles in a grid initially consisting of 256^3 cubic cells. Two cluster-sized halos from the $100 h^{-1} \text{ Mpc}$ box simulation and five MW-sized halos from the $12.5 h^{-1} \text{ Mpc}$ box simulation were selected for being resimulated with higher resolution. To increase resolution in the chosen halos, particles within 2.5 virial radii from the halo centers were traced back to the initial epoch and new initial conditions were then generated by using the multiple-mass scheme described in Klypin et al. (2001). Three different mass levels with 1, 8, and 64 times m_p were used, where m_p is the mass per particle at the finest mass level (see Table 1). Only parti-

TABLE 1

L_{BOX} ($h^{-1}\text{Mpc}$)	m_p ($h^{-1}M_\odot$)	Resolution ($h^{-1}\text{kpc}$)	σ_0 ($\text{cm}^2\text{gr}^{-1}$)	α	M_{vir} ($h^{-1}M_\odot$)	v_{max} (kms^{-1})	λ' (10^{-2})	N_{col}	Halo name tag
100.0	5.0×10^9	3.0	0.0	0.0	4.5×10^{14}	1280	4.43	0.00	<i>Cl1</i> _{0.0}
100.0	5.0×10^9	3.0	0.0	0.0	5.0×10^{14}	1230	1.80	0.00	<i>Cl2</i> _{0.0}
100.0	5.0×10^9	6.1	0.1	0.0	4.4×10^{14}	1285	4.57	0.60	<i>Cl1</i> _{0.1}
100.0	5.0×10^9	6.1	0.5	0.0	4.5×10^{14}	1299	4.88	2.37	<i>Cl1</i> _{0.5}
100.0	5.0×10^9	6.1	3.0	0.0	4.4×10^{14}	1336	4.62	12.54	<i>Cl1</i> _{3.0}
100.0	5.0×10^9	3.0	3.0	0.0	3.6×10^{14}	1548	2.17	30.03	<i>Cl2</i> _{3.0}
100.0	5.0×10^9	6.1	0.5	1.0	4.4×10^{14}	1276	4.47	0.35	<i>Cl1</i> _{0.5/V}
100.0	5.0×10^9	6.1	1.0	1.0	4.4×10^{14}	1270	4.45	0.64	<i>Cl1</i> _{1.0/V}
12.5	9.7×10^6	0.2	0.0	0.0	1.4×10^{12}	215	3.82	0.00	<i>G1</i> _{0.0}
12.5	9.7×10^6	0.2	0.0	0.0	2.7×10^{12}	237	7.21	0.00	<i>G2</i> _{0.0}
12.5	9.7×10^6	0.2	0.0	0.0	8.7×10^{11}	167	6.90	0.00	<i>G3</i> _{0.0}
12.5	9.7×10^6	0.4	0.1	0.0	1.3×10^{12}	214	4.18	0.33	<i>G1</i> _{0.1}
12.5	9.7×10^6	0.4	0.5	0.0	1.3×10^{12}	217	4.45	1.32	<i>G1</i> _{0.5}
12.5	9.7×10^6	0.4	0.5	0.0	2.6×10^{12}	240	7.45	...	<i>G2</i> _{0.5}
12.5	9.7×10^6	0.4	0.5	0.0	1.1×10^{12}	193	1.85	...	<i>G4</i> _{0.5}
12.5	9.7×10^6	0.4	0.5	0.0	1.1×10^{12}	178	5.53	...	<i>G5</i> _{0.5}
12.5	9.7×10^6	0.4	3.0	0.0	1.2×10^{12}	245	4.50	9.41	<i>G1</i> _{3.0}
12.5	9.7×10^6	0.1	3.0	0.0	2.3×10^{12}	273	5.70	15.03	<i>G2</i> _{3.0}
12.5	9.7×10^6	0.4	3.0	0.0	8.3×10^{11}	161	6.02	4.02	<i>G3</i> _{3.0}
12.5	9.7×10^6	0.4	0.5	1.0	1.3×10^{12}	212	4.28	0.77	<i>G1</i> _{0.5/V}
12.5	9.7×10^6	0.4	0.5	1.0	2.7×10^{12}	239	7.53	0.95	<i>G2</i> _{0.5/V}
12.5	9.7×10^6	0.4	1.0	1.0	1.3×10^{12}	212	4.31	1.34	<i>G1</i> _{1.0/V}

cles at this level were allowed to collide. Final halos have a few 10^5 particles each and contamination within their virial radii by heavy particles was kept below 1%. We notice that initial conditions do not change when σ_{DM} is varied.

The bound density maxima (BDM) group finding algorithm (Klypin et al. 1999) was used to identify halos and subhalos in all simulations. The BDM algorithm finds positions of local maxima in the density field smoothed at the scale of interest and applies physically motivated criteria to test whether a group of particles is a gravitationally bound halo. In the BDM algorithm, there is a parameter called the rejection velocity limit v_l which monitors whether a particle is bound or not. For standard CDM simulations, in which a virialized halo has a NFW like density profile, we usually set $v_l = v_e$, where the escape velocity v_e is analytically evaluated in BDM assuming the halo follows a NFW density profile. We decided to turn off the rejection velocity switch because density profiles of SIDM halos are not supposed to be fitted by a NFW profile. For subhalos the switch is kept on for two reasons: first, a significant fraction of unbound particles is expected to populate these subhalos, and second, because these halos are composed of at most hundreds of particles, their profiles in most cases are well fitted by a NFW profile.

2.3. Density Profiles

A summary of the parameters of the simulations of halos are presented in Table 1. The mass of the particle in the high-resolution region m_p is shown in column (2) and

is only a function of the size of the box (col. [1]) because the cosmological model and the number of mass levels are fixed. Column (3) shows the formal force resolution, measured by the size of a cell in the finest mesh. The collisionless CDM simulations have a higher resolution than the collisional ones because simulated halos in the former case reach a higher central density than in the latter one. Values of the parameters of the SI cross section, σ_0 and α , are presented in columns (4) and (5). The mass M_{vir} within the virial radius, defined as the radius at which the average halo density is δ times the background density according to the spherical top-hat model, is shown in column (6). δ is a number that depends on epoch and cosmological parameters (Ω_m, Ω_Λ); for a flat Λ CDM model, $\delta \sim 337$ at $z = 0$, where z is the redshift. The maximum circular velocity defined as

$$v_{max} = \left(\frac{GM(< r)}{r} \right)_{max}^{1/2}, \quad (3)$$

where G is the gravitational constant and $M(< r)$ is the mass contained within the radius r , is placed in column (7). The spin parameter λ' as defined by Bullock et al. (2001) is shown in column (8) (see §3.4). In column (9) N_{col} denotes the total number of collisions until $z = 0$ divided by the total number of particles within R_{vir} ; as mentioned above, only particles at the finest mass-level of refinement are allowed to collide. This number could not be obtained for those halos (horizontal dots) that were simulated simultaneously in only one run because the col-

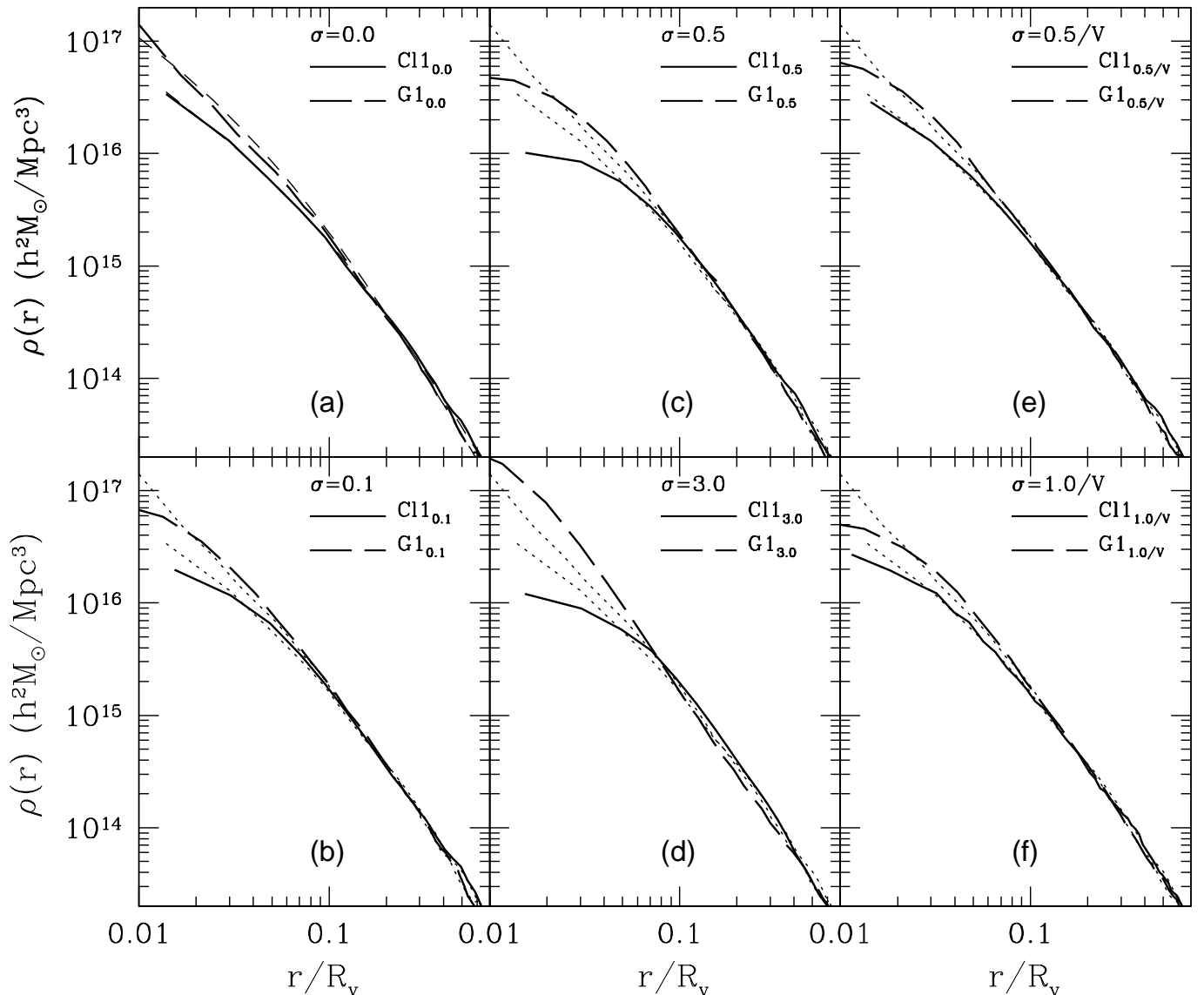


FIG. 3.— Density profiles of the fiducial cluster- (solid lines) and MW-sized (dashed lines) halos simulated with different values of σ_{DM} (see top of each panel). V is the v_{12} in unities of 100 km s^{-1} . Dotted curves are the profiles of the CDM case (panel a) plotted for comparison. Dashed curves in panel (a) are the best NFW fit to the profiles shown there. Radius is given in unities of the virial radius R_{vir} .

lision counting refers to the whole region selected to be resimulated at high resolution. In column (10) we give the halo name tag for each one of the simulated halos. Labels Cl_n denote cluster-sized halos (n goes from 1 to 2), whereas labels Gn denote MW-sized halos (n goes from 1 to 5). The numbers $n = 1, 2$ for halos Cl , and $n = 1, 2, 3$ for halos G indicate different simulations aimed to have halos with different mass assembly histories. MW-sized halos numbers 4 and 5 turned to appear in the same simulation as the halo $G2$, and we have included them for completeness. Both, the cluster- and MW-sized halos have been simulated for a variety of (σ_0, α) values; the lower index in the name tag indicates the used combination. Note

that only halos with $n = 1$ were simulated with all the six (σ_0, α) pairs of values; they are our fiducial halos.

3. HALO STRUCTURE

The six panels of Figure 3 show the density profiles of the fiducial cluster-sized halo ($Cl1$, solid lines) and MW-sized halo ($G1$, long-dashed lines) for the different (σ_0, α) pair values considered here. The fiducial halos $G1$ and $Cl1$ were selected in the low-resolution CDM simulations with concentrations typical for their masses in an attempt to simulate halos with typical MAHs, since it is known that the concentration of the halo is related to its MAH (Avila-Reese et al. 1998, 1999; Wechsler et al. 2001). Un-

fortunately, in the high-resolution CDM simulation, the halos turned out to be more concentrated ($c_{\text{NFW}} = 10$ instead of 6, and $c_{\text{NFW}} = 17.2$ instead of 13, respectively). Besides, a major merger in the halo *Cl1* that occurs at $a < 1$ in the low-resolution CDM simulation is delayed to $a \gtrsim 1$ in the corresponding high-resolution simulation; this will shift the core collapse phase to an epoch $a > 1$ when $\sigma_{DM} = 3.0 \text{ cm}^2\text{gr}^{-1}$, as we will discuss below. In Figure 3, for reference, the density profiles of the two CDM models shown in panel (a) are also plotted with dotted lines in the other panels. The best NFW fits to the CDM profiles are shown with short-dashed lines in panel (a).

From a first inspection of Figure 3, we conclude that significant differences in the density profiles (flattening) among the halos with different values of (σ_0, α) apply only to those regions with radii smaller than $0.03 - 0.05 R_{\text{vir}}$. The exception are the halos with $(\sigma_0, \alpha) = (3.0, 0.0)$; in this case SI affects dramatically the inner structure at radii even larger than $0.05 R_{\text{vir}}$. The parameter which defines the evolution under SI is the number of collisions per particle after a given time t ,

$$N_{\text{col}} \propto \rho \langle \sigma_{DM} |v_{12}| \rangle t \propto \rho \sigma_{DM} \sigma_{3D} t, \quad (4)$$

where σ_{3D} is the 3D velocity dispersion. The maximum σ_{3D} is proportional to v_{max} . From all of our runs we see that if N_{col} at the present epoch is smaller than $\approx 2 - 5$ (see Table 1), then the halo is either in the core expansion phase or has just had the gravothermal catastrophe triggered, being the core shrinkage still negligible. When σ_{DM} is constant, the cores of low velocity halos are on average less influenced by SI than the high velocity ones. On the other hand, when $\sigma_{DM} \propto 1/v_{12}$, we expect halos of different sizes to have roughly similar core densities. These predictions are closely obeyed as seen in panels (b), (c), and panels (e) and (f) of Figure 3, respectively, or in Figure 4 below. Nevertheless, this simple reasoning applies strictly only for monolithic halos. The cosmological merger history may dramatically influence the $z = 0$ structure of halos with significant SI. This is the case of the cluster-sized halo in the simulation with $\sigma_{DM} = 3.0 \text{ cm}^2\text{gr}^{-1}$, *Cl1*_{3.0} (panel d). This halo should have evolved faster under the influence of SI than the MW-sized halo *G1*_{3.0}. However, this did not happen; while halo *G1*_{3.0} is in an advanced stage of core collapse, halo *Cl1*_{3.0} is just entering into this phase. The core collapse in the latter case seems to have been delayed by a recent major merger. We have simulated a second cluster-sized halo with $\sigma_{DM} = 3.0 \text{ cm}^2\text{gr}^{-1}$, *Cl2*_{3.0}, which does not suffer late major mergers. The core collapse phase at $a = 1$ in this halo is well advanced and its central density and concentration are higher than those of the corresponding MW-sized halo (see Fig. 4 below).

An important effect to note is that the core evolves fast after it reaches its maximum expansion. The central density as well as N_{col} (see eq. 4) increase quickly. This is why N_{col} at $z = 0$ for the halo *G1*_{3.0} is similar to that of the halo *Cl1*_{3.0} (see Table 1) despite that the latter has a v_{max} 5.5 times larger than the former. We recall that halo *Cl1*_{3.0} delayed its core collapse due to a late major merger. Owing to the transient nature of the SIDM halo cores, a comparison of core parameters at a given epoch (e.g., $z = 0$) for different values of σ_{DM} and different halos

masses and MAHs may lead to misleading conclusions.

In the following, we analyze in more detail the density profiles of the cluster and MW-sized SIDM halos in the light of previous works and then explore the influence of the MAH on their evolution.

3.0.1. Cluster-sized halos

As mentioned above, it turned out that the chosen cluster-sized halo, which in the low-resolution CDM simulation was relaxed at $a = 1.0$ ($a = 1/(1+z)$), is in the high-resolution simulation about to suffer a major merger. The time when this merger happens seems to be a function of σ_{DM} . We find that the halo *Cl1* with $(\sigma_0, \alpha) = (3.0, 0.0)$ suffers this merger before it reaches the present time, while *Cl1* halos with other σ_{DM} values suffer this merger soon after $a = 1.0$. This is why in Figure 3 we compare the density profiles of halos *Cl1* at time $a = 1.1$, an epoch when the *Cl1* halos with different values of σ_{DM} have already experienced their last major merger.

We find the same general trend observed by Yoshida et al. (2000b) at $z = 0$: as σ_{DM} increases, the core radius, $r_{c,-1}$, defined in this paper as the radius where density profile slope becomes steeper than -1 , increases and the central density, $\rho_{c,-1}$, decreases. However, differences between Yoshida et al. results and ours do exist: in our simulations there is a σ_{DM} (for the constant σ_{DM} case) for which the trend is reversed. For example, $r_{c,-1}$ for halo *Cl1*_{3.0} is not greater than the corresponding $r_{c,-1}$ of halo *Cl1*_{0.5}, and for halo *Cl2*_{3.0}, $r_{c,-1}$ is even much smaller. The trend of the core radius or central density with σ_{DM} at $z = 0$ is reversed owing to the core collapse. The halo with $\sigma_{DM} = 10.0 \text{ cm}^2\text{gr}^{-1}$ of Yoshida et al. is also undergoing a core collapse; however, at $z = 0$ the central density of this halo is still larger than the central density of their halo simulated with $\sigma_{DM} = 1.0 \text{ cm}^2\text{gr}^{-1}$. Is the rate at which the core shrinks and the central density grows up in the stage of core collapse slower in their case than in ours? We have measured this rate in both their cluster and our cluster halo *Cl1*_{3.0} and have found that the rates are actually similar. The difference between ours and Yoshida's et al. results may be found in the minimum central density reached by the halos. In their case, this density is lower than in our case by a factor of three. This is probably why the soft core at $z = 0$ of their cluster halo simulated with $\sigma_{DM} = 10.0 \text{ cm}^2\text{gr}^{-1}$ have not become yet smaller than the corresponding one to the simulation with $\sigma_{DM} = 1.0 \text{ cm}^2\text{gr}^{-1}$, in contrast to our results where for $\sigma_{DM} = 3.0 \text{ cm}^2\text{gr}^{-1}$ the soft core is already smaller than for $\sigma_{DM} = 0.5 \text{ cm}^2\text{gr}^{-1}$.

Since halo *Cl1*_{3.0} assembles most of its mass through late major mergers, the triggering of the core collapse phase, which is almost inevitably present in almost all halos with $(\sigma_0, \alpha) = (3.0, 0.0)$, is delayed, and at $a = 1.1$ still has a prominent soft core, although it is already shrinking because of the core collapse. After the last major merger took place, little mass is accreted by the halo in the next 3.5×10^9 yr; it is thus tempting to compare the core evolution since that epoch with the predictions of the monolithic case of KW. The halo *Cl1*_{3.0} would have a $\hat{\sigma}$ that lies in the interval $[3.5, 4.0]^2$ and a dynamical time t_{dyn} , as defined by KW, of 1.7×10^9 yr. From $a = 0.85$, which is the epoch

²Aside from σ_0 we also need to know the concentration and the total mass in order to compute $\hat{\sigma}$. We have taken these parameters from

where the maximum core expansion occurs, to $a = 1.10$ we see that the core shrinks by a factor of 1.3. KW predict for this model a shrinking factor of about 1.4-1.5. It is not clear how far we can take the comparison of the SIDM cosmological scenario with the monolithic case, but here we have a case in which consistent results are obtained.

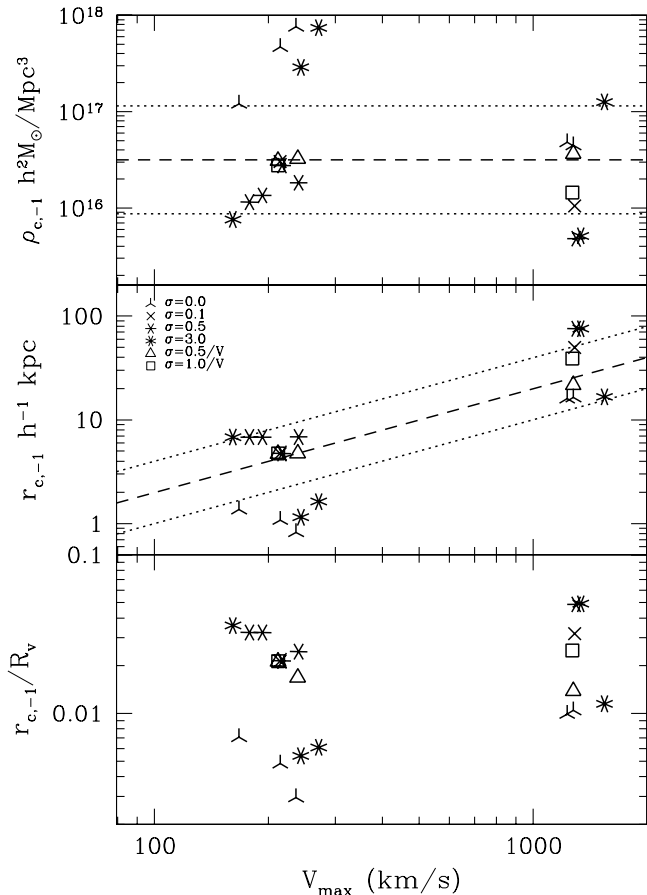


FIG. 4.— Central density, core radius and core fraction vs. v_{\max} for cluster- and MW-sized halos simulated here for different values of σ_{DM} (see the corresponding symbols in the middle panel; σ_{DM} is in units of $\text{cm}^2\text{gr}^{-1}$ and V is v_{12} in units of 100 km s^{-1}). Central density $\rho_{c,-1}$ and core radius $r_{c,-1}$ are defined as the density and radius where the profile slope becomes steeper than -1 , respectively. Dashed and dotted lines in the two upper panels are the average and the $2 - \sigma$ dispersion inferred from observations of dwarf and LSB galaxies and cluster of galaxies (see §5.2 for details).

3.0.2. Milky Way-sized halo G1

The fiducial MW-sized halo G1 resulted more concentrated (see above) and with a MAH more biased to an early halo-assembly than the average corresponding to its mass. Moreover, the late MAH of this halo is nearly smooth, without violent major mergers since $a = 0.5$.

The non-monothonic trend of the core radius or the central density with σ_{DM} at $z = 0$ slightly outlined by the

its correspondent CDM cluster halo. This is a good approximation because once the cluster forms, which we can establish at the last major merger, the parameter r_{NFW} does not change much.

³We later realized that what matters is not only the amount of mass but how this mass is accreted. Smooth infall of material to halo outskirts does not seem to alter significantly the dynamical core SI evolution

fiducial cluster-sized halo is clearly present in the fiducial MW-sized halo (Fig. 3). This is much better appreciated in Figure 4. Here we plot v_{\max} versus central density, $\rho_{c,-1}$, measured at the radius $r_{c,-1}$ where the profile slope becomes steeper than -1 (a), the core radius, $r_{c,-1}$ (b), and the core radius fraction, $r_{c,-1}/R_{vir}$, (c). Note that halos with $(\sigma_0, \alpha) = (0.1, 0.0)$ and $(0.5, 0.0)$ tend to lie in the same region; i.e., an increase in σ_0 does not necessarily produce an increase in core radius at $z = 0$. In the framework of a monolithic halo this could be explained as follows: because the core relaxation time for halos with $(\sigma_0, \alpha) = (0.1, 0.0)$ is close or greater than the Hubble time, we still find these halos in their core expansion phase at the present time, whereas halos with $(\sigma_0, \alpha) = (0.5, 0.0)$ are at the onset of the core collapse phase. These facts conspire to give similar core parameters in both cases. Halo G13.0 on the other hand, is well inside the core collapse phase and this is why $r_{c,-1}$ is small. It is interesting to note that SI introduces a peculiar epoch in the history of the universe at which the dark halos change their inner structure from an extended smooth core to a very cuspy center. For the case $\sigma_{DM} \propto 1/v_{12}$, this epoch does not depend too much on the halo mass or v_{\max} , and it is determined mainly by the value of σ_0 . However, violent mergers and other effects may delay significantly the core collapse phase for some halos and subhalos (see §3.1.3).

In Figures 5 and 6 we plot the evolution of the density and 3D velocity dispersion profiles, and of the heat capacity profile, respectively, of the core collapsing halo G13.0 from $a = 0.4$ to $a = 1.0$ (left panels). Proper units were used. As in the case of halo G113.0, one could ask whether the strong evolution of ρ_c is expected or not. To address this question we first notice that only 20% of the present total mass is accreted since the last major merger, which occurs at $a \simeq 0.5$. Therefore, treating the evolution of this halo from $a = 0.5$ to $a = 1$ as an isolated case seems to be a fair approximation³. As we did for the fiducial cluster-sized halo, we compute the corresponding $\hat{\sigma}$ and dynamical time; they are 1.9 and 6.4×10^8 yr, respectively. From the KW simulations of monolithic halos, this model changes its core radius by a factor of four in approximately $5-6t_{dyn}$; this same change is seen in halo G13.0 but in about $10t_{dyn}$. We can explain this difference in the core evolution rate as being due to the infalling and merging material in the cosmological halo. This also could explain why the inner region where the heat capacity C is positive increases during the expansion phase in halo G13.0 (Fig. 6) unlike what happens with the monolithic halo in §2.1 (Fig. 1). The subsequent core collapse phase is characterized by a reduction of the region where $C > 0$.

The core collapse of halo G13.0 (and G23.0, see below) is at odds with the results of Davé et al. (2001). They ran a simulation of 128^3 particles in a $4 \text{ h}^{-1}\text{Mpc}$ box for the same cosmological parameters used here. Their power spectrum is normalized to $\sigma_8 = 0.8$. The most massive halo formed in their simulation has a mass of $6.2 \times 10^{11} M_\odot$ and consists of about 1.7×10^5 particles. None of the halos in the two SI models that they consider, $(0.56, 0.0)$ and $(5.6, 0.0)$, shows signs of being in the core collapse phase.

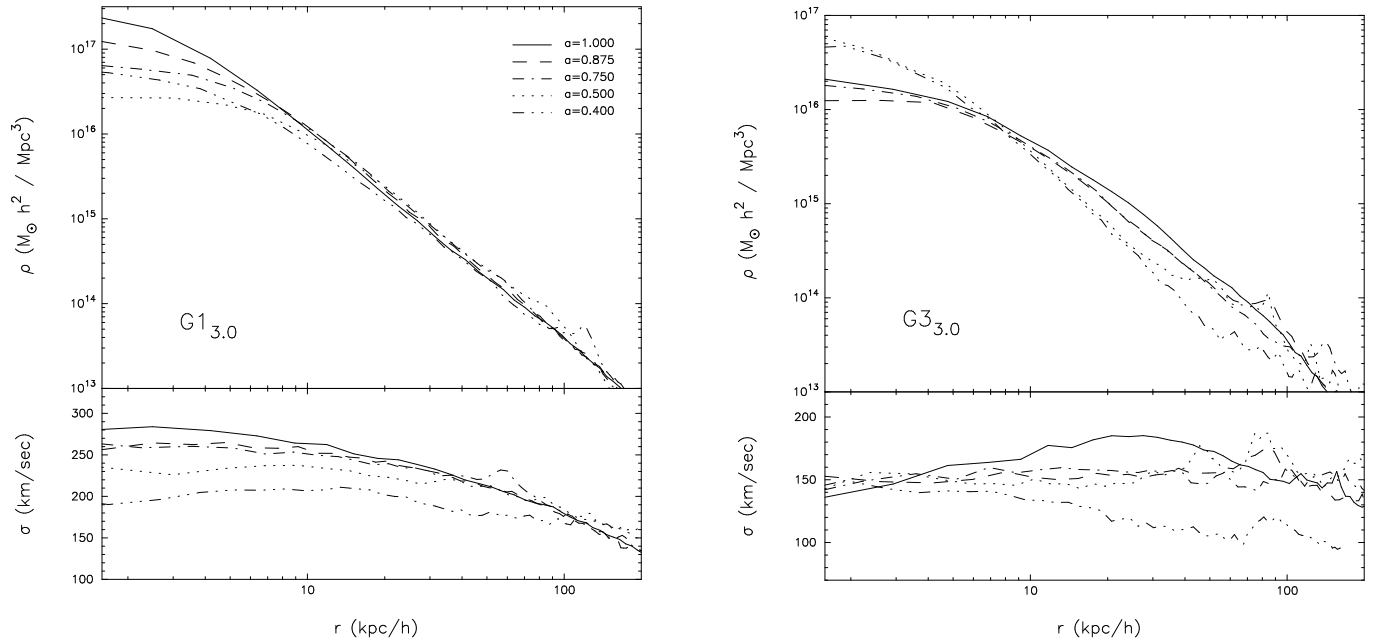


FIG. 5.— Evolution of the density and the 3D velocity dispersion profiles of the $G1$ (left) and $G3$ (right) halos in proper units and for $(\sigma_{DM}, \alpha) = (3.0, 0.0)$. In both halos the core reaches its maximum size a little later after the major merger occurs, around $a = 0.5$ for $G1_{3.0}$ and $a \simeq 1.0$ for $G3_{3.0}$; for times earlier than this, the central densities of the major progenitors of the halos are higher. The shape of the density profiles of their corresponding CDM halos do not change after the major mergers occur, the subsequent infall of material serves essentially to increase the proper size of the halo. Because a very small amount of material reach the core (see also the paper by Zhao et al. 2002), we can safely say that the inner regions of the SI halos evolved as if they were isolated; in other words, the number of collisions inside the core overwhelms the number of particles that fall into it. So, it is not very surprising, after all, that we also see a core collapse in MW-sized *cosmological* halos.

On the contrary, the halos have extended shallow cores which increase as σ_{DM} increases. Davé et al. suggested that the accretion of dynamically hot material, intrinsic to the CDM cosmological simulations, is so important to the halo core evolution that predictions for SIDM from monolithic halos does not apply at all to the cosmological setting.

3.0.3. Halos with different assembling histories

In the following, we test the possibility that our differences with Davé et al. (2001) might reside in the halo MAHs. It is well known that CDM halos form from a variety of MAHs which give rise to a variety of present-day structures (e.g., Avila-Reese et al. 1998,1999). As mentioned above, the fiducial halo assembled early and ended highly concentrated. We need to simulate now a halo with a low concentration and a late halo-assembly. We chose two MW-sized halos with these characteristics, $G2_{0.0}$ and $G3_{0.0}$, from the same low-mass resolution simulation as the one from which the halo $G1_{0.0}$ was taken; $G2_{3.0}$ and $G3_{3.0}$ are the corresponding SI halos with $(\sigma_0, \alpha) = (3.0, 0.0)$. As for the fiducial halo, in the high resolution simulation the halos resulted with a higher concentration and a less extended MAH than in the low resolution one. In any case, both halos are less concentrated and have a more extended MAH than the fiducial one.

To our surprise, halo $G2_{3.0}$ also undergoes a fast core

collapse, no matter that this halo accretes a little more than half of its present mass from $a = 0.5$ to $a = 1.0$! An analysis of the MAH of the corresponding CDM halo shows that the last major merger occurs as early as $a \simeq 0.3$; after this epoch the mass is accreted *smoothly* and/or in small chunks. A recent paper by Zhao et al. (2002) shows that the build-up of CDM halos can be divided in time in two phases: an early one characterized by violent mergers in which the inner halo density profile is significantly altered, and a late one characterized by a smooth accretion of material in which the accreted material retains its low binding energy and is added to the outer part of the halo. Depending on the MAH, a halo can go from one phase to the other early or late in time. Halos $G1_{0.0}$ and $G2_{0.0}$ appear to have typical transition epochs, although the latter accretes (smoothly) much more mass at late epochs than the former one. On the other hand, halo $G3_{0.0}$ seems to have the transition at $z \simeq 0$. This halo assembles most of its mass by recent major mergers.

Besides of the direct dynamical effect of the mergers on the structure of halo $G3_{3.0}$, its core collapse may be delayed by conduction effects. The major mergers heat the halo periphery, producing an increment of the outer velocity dispersion (temperature), as it seen in the right panel of Fig. 5 (dotted line). In this case, the halo at $a = 0.4$ was already starting its core collapse phase. The heat capacity also increases due to the major mergers (Fig. 6). Then,

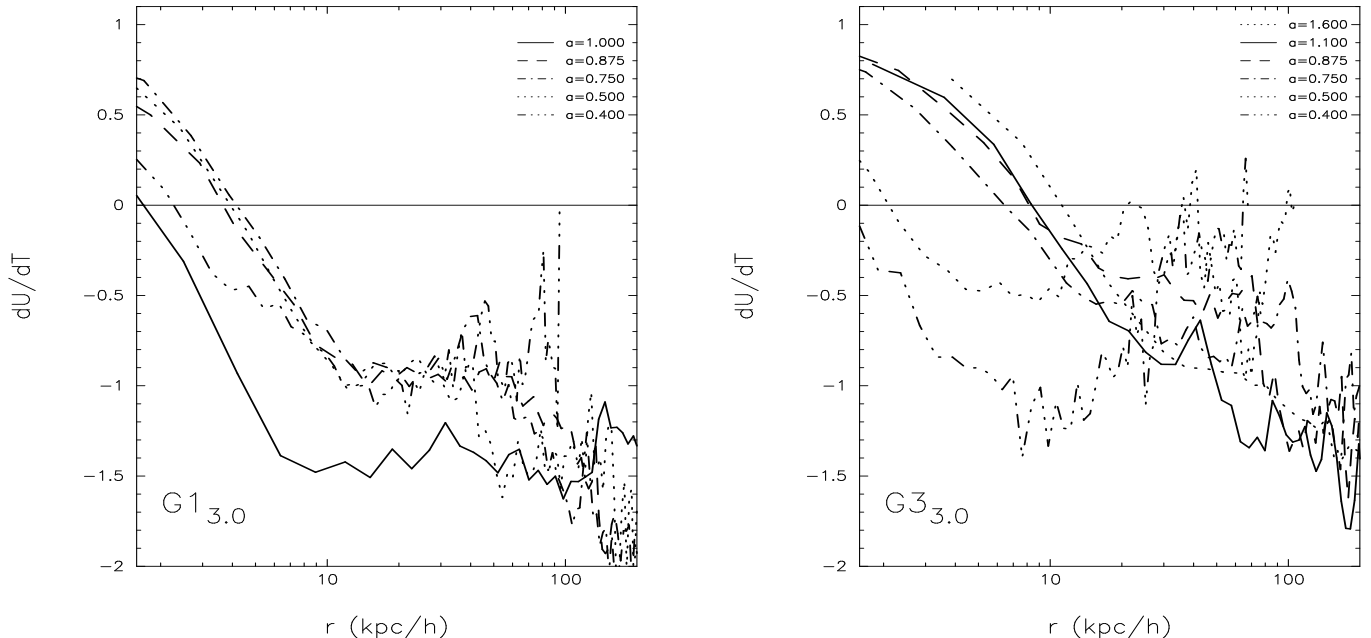


FIG. 6.— Evolution of the heat capacity, $C \equiv dU/dT$, profiles for halos $G1_{3.0}$ (left panel) and $G3_{3.0}$ (right panel). Notice how the size of the region where heat capacity is positive increases in both halos as the cores of the halos approach their maximum radius. As the core collapse proceeds in halo $G1_{3.0}$ the region where C is positive shrinks. This is different to what we see in the subsequent evolution of C in halo $G1_{3.0}$, where the core collapse is absent; in this case the size of the $C > 0$ region even increases as time passes.

heat starts flowing into the $C > 0$ core and produce its expansion (see §2.1). This process may last a significant period of time, until the heat conduction isothermalise most of the halo. We let the simulation of halo $G3_{3.0}$ run for another Hubble time and to our surprise even at $a = 1.6$, about 20 Gyr after the Big Bang, the halo has not undergone a core collapse and the heat capacity increased even slightly. We should note that this halo is also peculiar because close to it there is a galaxy-sized more massive halo. We notice, on the other hand, that because halo $G3_{3.0}$ is smaller ($v_{\max} = 163 \text{ km s}^{-1}$) than halos $G1_{3.0}$ and $G2_{3.0}$, we expect the SI evolution of this halo to be slower than that of halos $G1_{3.0}$ and $G2_{3.0}$.

Our results show that, for both the cluster- and MW-sized halos with $(\sigma_{DM}, \alpha) = (3.0, 0.0)$, the core collapse is delayed until the stage of *major mergers* ends. We further simulated the halo $G1$ with a still higher σ_{DM} ($= 10.0 \text{ cm}^2 \text{ gr}^{-1}$) and check, in fact, that the core collapse begins only after the last major merger. Therefore, we conclude that the dynamics of SIDM halos with a high cross section is strongly affected by *violent merging processes rather than by smooth mass aggregation*. A continuous injection of “dynamical heat”, able to either heat and expand directly the core or rise the temperature of the halo periphery to above the core’s temperature, seems to be possible only when the halo grows by violent mergers. In summary, when SI is efficient ($\sigma_{DM} = 3.0 \text{ cm}^2 \text{ gr}^{-1}$, for example) the inner structure of halos may depend strongly on the halo

merging history. The onset of the core collapse phase occurs immediately after the core relaxes, in agreement with the finding of KW (see also Quinlan 1996; Burkert 2000), but this process can be delayed by subsequent major mergers as we actually see in some of our halos. Can this explain our differences with Davé et al. (2001) results?

3.1. Concentrations

A more quantitative way to measure differences in the structure among halos is using concentration parameters. In Figure 7 we plot the $c_{1/5}$ and c_M concentration parameters⁴ versus virial mass M_{vir} for halos (large symbols) and subhalos with more than 1000 particles (small symbols) from our different simulations. To avoid too much overlapping, we divided Figure 7 in two sequences of panels. Halos with $(\sigma_0, \alpha) = (0.0, 0.0)$, $(0.1, 0.0)$, $(3.0, 0.0)$, and $(1.0, 1.0)$ are shown in left panels while halos with $(\sigma_0, \alpha) = (0.5, 0.0)$ and $(0.5, 1.0)$ are shown in right panels. We also plot in Figure 7 the density measured at $0.03R_{vir}$ ($\rho_{c,.03}$) versus M_{vir} . Because our high-resolution simulations were designed to be focused on a specific (cluster- or MW-sized) halo, most subhalos lie within the virial radii of these halos (satellites). The mass of subhalos is defined as the minimum between the virial mass and the truncated mass (see Avila-Reese et al. 1999).

From Figure 7 one sees that halos with different (σ_0, α) values have similar $c_{1/5}$ parameters, except for halos $G1_{3.0}$ and $G2_{3.0}$, in which the region where $1/5$ th of M_{vir} is con-

⁴ $c_{1/5}$ is defined as the ratio between the virial radius R_{vir} and the radius where $1/5$ of the total halo mass is contained (Avila-Reese et al. 1999). c_M is defined as 27 times the ratio between the mass at $r_{in} = 8.5 \text{ kpc } v_{\max}/220 \text{ km s}^{-1}$ and the mass at $r_{out} = 3 \times r_{in}$ (Dave et al. 2001). These definitions of the concentration parameter are independent from the particular fitting applied to the halo density profile.

tained is greatly affected by the core collapse, and halo $G3_{3.0}$, whose peculiar MAH makes it keep a relatively long-lived shallow core (see §3.1.3). A similar behavior is observed for $\rho_{c,.03}$. The parameter c_M reflects with better accuracy the inner matter distribution of halos. Note that the c_M parameter of subhalos with more than 1000 particles from the MW-sized $(\sigma_0, \alpha) = (0.5, 0.0)$ simulations are similar to those from the $(\sigma_0, \alpha) = (0.56, 0.0)$ simulation of Davé et al. (2001). Halos with higher σ_0 have smaller c_M concentrations, for a given α . Again, this trend can be reversed at the high σ_0 end because of the core collapse. Subhalos follow roughly the same behavior of halos in all the three parameters of Figure 7 as a function of mass. However, before drawing any conclusion we should bear in mind that (i) subhalos are resolved only with hundreds of particles and (ii) that they can result strongly affected by the self-interacting environment of the halo where they are embedded.

The lack of mass resolution does not allow us to explore in detail the effect of SI on the inner dynamics and structure of subhalos. In order to evaluate this problem, we analyze the MW-sized halos obtained in a low resolution (64^3 particles) simulation with $(\sigma_0, \alpha) = (3.0, 0.0)$. This is the same simulation from where MW-sized halos were taken. The SIDM MW-sized halos in this simulation have only few thousands of particles and we find that their inner structures are not at all similar to those of their high-resolution counterparts. Therefore, we can not be conclusive about the inner structures of the subhalos in the high-resolution simulations presented here because they have at the most only a few thousands of particles. Nevertheless, our simulations allow us to explore the effect the hot particles of the host halo has on the overall structure of subhalos. The $c_{1/5}$, c_M , and $\rho_{c,.03}$ parameters of the subhalos from the cluster-sized halo simulation $C1_{3.0}$ are smaller than those same parameters of the isolated MW-sized halos from the low resolution simulation. In both cases the halo masses and number of particles are similar. This difference seems to have only one explanation: the structure of subhalos (satellites) is affected by the environment of the hot host halo. Subhalo particles are being ejected continuously because high speed particles from the hot host halo collide with the cooler subhalo particles, exchanging orbital energy by internal energy; in the extreme case, the subhalo can be evaporated completely (Gnedin & Ostriker 2002). The survivor subhalos are indeed “puffy” with density profiles much flatter than the isolated halos.

More evidence about the influence of SIDM halos on the structure of their subhalos comes from comparing subhalos of simulation $G1_{1.0/V}$ with subhalos of simulation $G1_{3.0}$ (Fig. 7). Subhalos from the former simulation (squares) have an effective σ_{DM} of $\approx 3 - 5 \text{ cm}^2\text{gr}^{-1}$, i.e., similar to the σ_{DM} of the latter simulation (lowest starred symbols); however, they are located in different regions in Figure 7 (the same happens for subhalos with less than 1000 particles). The difference between both simulations is in the effective σ_{DM} value of the host halos: $\sim 0.5 \text{ cm}^2\text{gr}^{-1}$ versus $3 \text{ cm}^2\text{gr}^{-1}$, respectively. The evaporation effect of the hot SIDM halo $G1_{3.0}$ is stronger than the one of the halo $G1_{1.0/V}$; in fact, in the former case most subhalos have been destroyed by the present time (see §4). A similar effect is observed

in subhalos from the $(\sigma_0, \alpha) = (0.5, 1.0)$ and $(0.5, 0.0)$ simulations. For the MW-sized halos of the former simulation, the effective value of σ_{DM} is $\approx 0.2 \text{ cm}^2\text{gr}^{-1}$ while for their subhalos it is $\sigma_{DM} \approx 1.5 - 3.0 \text{ cm}^2\text{gr}^{-1}$; i.e., 3-6 times larger than for subhalos of the latter simulation. Despite the relatively high value of σ_{DM} of subhalos in the $(0.5, 1.0)$ model, their structures look similar to their CDM counterparts (low-mass resolution does not allow SI to work properly). However, subhalos from the simulation with $\sigma_{DM} = 0.5 \text{ cm}^2\text{gr}^{-1}$ are “puffier” than those subhalos from CDM (right panels, Fig. 7). This can also be explained by an action of the hot halo environment on the dynamics of subhalos.

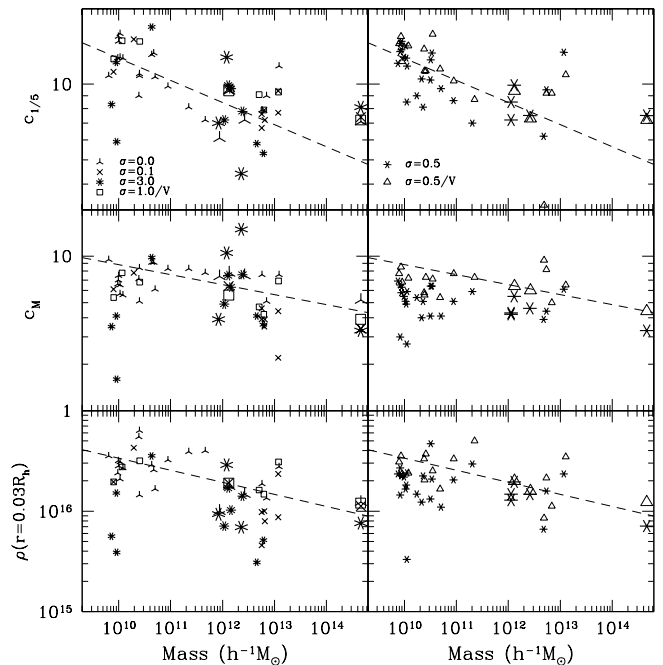


FIG. 7.— Concentration parameters $c_{1/5}$ and c_M , and density $\rho_{c,.03}$ at $0.03R_{vir}$ versus halo mass for halos (large symbols) and guest halos with more than 1000 particles (small symbols) from simulations with different values of σ_{DM} (see the corresponding symbols in upper panels; same unities as in Fig. 3). Results were divided in two sequences of panels in order to avoid too much overlapping. Tiny starred symbols in the left panels are for the low-mass resolution simulation in the $12.5 \text{ h}^{-1}\text{Mpc}$ box with $(\sigma_0, \alpha) = (3.0, 0.0)$. Their structural properties are different to that of their high-mass resolution counterparts (bright starred symbols). Dashed line in the upper panels is the linear regression found in Avila-Reese et al. (1999) for isolated ACDM halos in a $60 \text{ h}^{-1}\text{Mpc}$ box. Dashed line in medium and lower panels are estimates of the $c_M - M_{vir}$ and $\rho_{c,.03} - M_{vir}$ relations for isolated ACDM halos from the the same simulation of Avila-Reese et al. (1999). c_M was calculated from c_{NFW} using Fig. 6 in Davé et al. (2001).

3.2. Ellipticities

Another prediction by the SIDM cosmology is that the halo inner region, where a shallow core forms, should be close to spherical because collisions tend to reduce the degree of anisotropy.

We have measured the ellipticities of halos using the

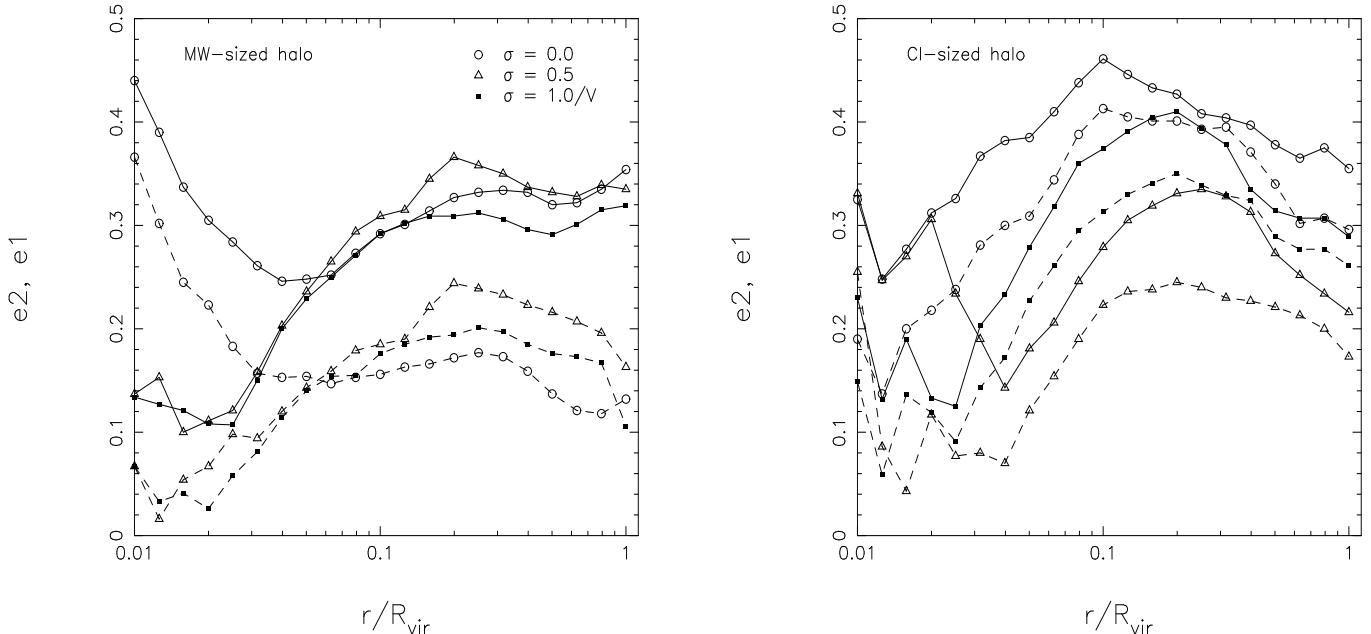


FIG. 8.— Ellipticities e_1 and e_2 as a function of radius are shown in left (halo *G1*) and right (halo *CI1*) panels. As expected, SI halo are rounder than the corresponding CDM halos, being the effect greater for the cluster-sized halo.

tensor of inertia. This is defined as

$$I_{i,j} = \sum x_i x_j / r^2, \quad (5)$$

where the sum is over all particles within r_{vir} , x_i ($i = 1, 2, 3$) are the particle coordinates with respect to the halo center of mass, and r is the distance of the particle to the halo center. The ellipticities are then given by

$$e_1 = 1 - \frac{\lambda_1}{\lambda_3}, \quad e_2 = 1 - \frac{\lambda_2}{\lambda_3}, \quad (6)$$

where $\lambda_3 > \lambda_2 > \lambda_1$ are the eigenvalues of the tensor of inertia. We evaluate the triaxiality parameter using the following formula (e.g., Franx, Illingworth, & de Zeeuw 1990)

$$T = \frac{\lambda_3^2 - \lambda_2^2}{\lambda_3^2 - \lambda_1^2}. \quad (7)$$

A halo is prolate (oblate) if $T = 1.0$ ($T = 0.0$).

The ellipticities e_1 and e_2 as a function of radius are shown in Figure 8 for our fiducial MW- and cluster-sized halos for three models $\sigma_{DM} = 0.0, 0.5$, and $1.0/V \text{cm}^2 \text{gr}^{-1}$. We have denoted with solid and dashed lines e_1 and e_2 , respectively. We see, as expected, that the differences in the ellipticities between SI and CDM halos are found in the inner parts. At large radii, the difference in e_1 or e_2 values among the plotted MW-sized halos is lower than the difference between the values of the ellipticities e_1 and e_2 . The opposite occurs for the cluster-sized halo. Note, moreover, that unlike *G1* halos, SI *CI1* halos are rounder at all radii.

Cores of SI halos are indeed rounder than their CDM counterparts, but they are not spherical. Unfortunately, ellipticities in real galaxies are ill determined, so it is not

clear how much we can constrain the SI parameters with this kind of observations. Miralda-Escudé (2002) claims, however, to have constrained the constant cross section to be less than $\simeq 0.02 \text{cm}^2 \text{gr}^{-1}$ with the determination of the ellipticity of cluster MS 2137-23 through a lensing study. The question remains whether the ellipticity he derives for MS 2137-23 does disagree with the one found in a typical cluster-sized *simulated halo* with $\sigma_{DM} > 0.02 \text{cm}^2 \text{gr}^{-1}$. We let this analysis for a subsequent paper.

3.3. Angular Momentum Distribution

For each halo we compute the total angular momentum as

$$\mathbf{J} = m_i \sum_{i=1}^n \mathbf{r}_i \times \mathbf{v}_i, \quad (8)$$

where \mathbf{r}_i and \mathbf{v}_i are the position and velocity of the i th particle with respect to the halo center of mass. We follow Bullock et al. (2001) and define a modified spin parameter λ' to characterize the global angular momentum of a halo

$$\lambda' \equiv \frac{J_{vir}}{\sqrt{2} M_{vir} V_{vir} R_{vir}}, \quad (9)$$

where J_{vir} is the angular momentum inside the virial radius R_{vir} , and V_{vir} is the circular velocity at radius R_{vir} . In Table 1, column (8), we show λ' for all of our halos. Notice that λ' increases with σ_{DM} in both cluster- and MW-sized halos for constant σ_0 , from $\sigma_0 = 0.0$ to 0.5 . Nevertheless, this effect is small, amounting to 10%, 16% and 3% for halos *CI1*, *G1* and *G2*, respectively. It measures roughly the difference in the number of particles with low angular momentum in inner regions between CDM and SI halos. Moreover, for those halos for which $\sigma_{DM} \propto 1/v_{12}$, the effective σ_{DM} is so small that a factor of two of change in σ_0 passes unnoticed by λ' .

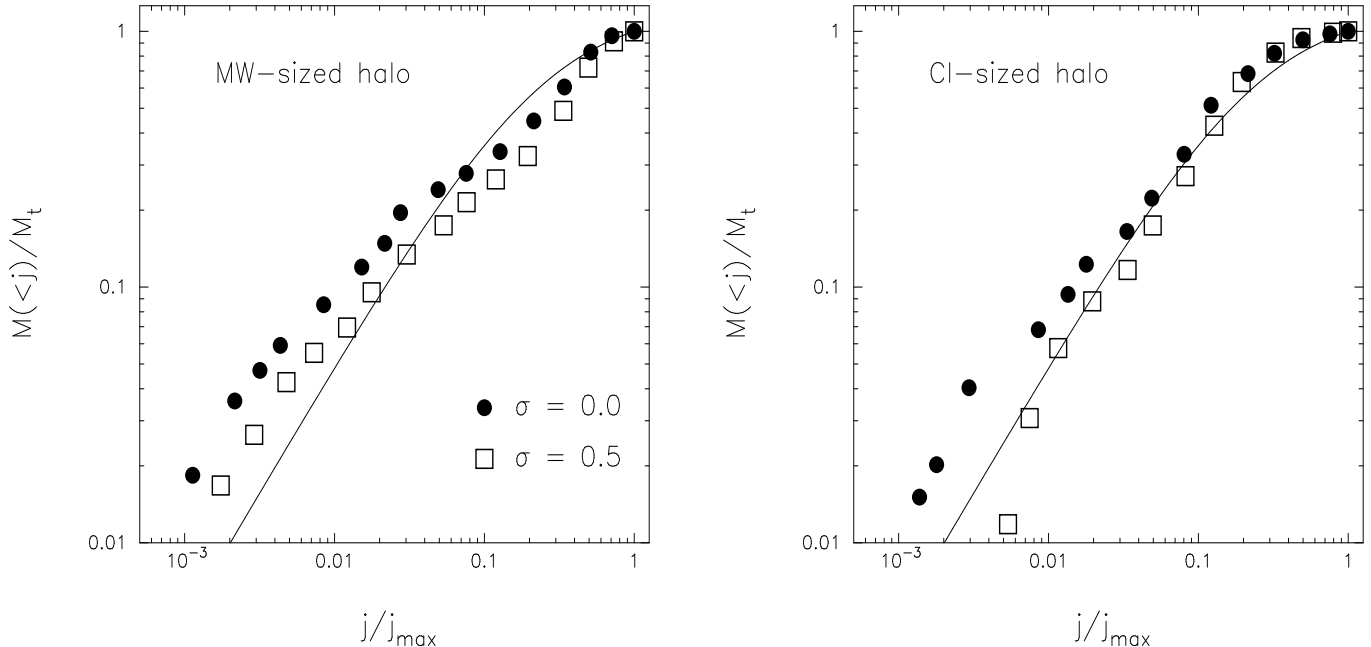


FIG. 9.— Specific angular momentum j distribution for halos $G1_{0.0}$ (circles) and $G1_{0.5}$ (squares) panel (a) and for halos $Cl1_{0.0}$ (circles) and $Cl1_{0.5}$ (squares) panel (b). Only cells with positive j were considered and the total mass M_t was redefined to be the mass contained in all those cells with positive j . The line is taken from the analytical fit of Bullock et al. (2001) $m(<j) = \mu \tilde{j}/1 + \tilde{j}$, where $m(<j) \equiv M(<j)/M_{vir}$ and $\tilde{j} \equiv j/j_{max}$, with $\mu = 1.25$. Notice that differences between the CDM and SI $m(<j)$ profiles are only at the low- j end. We see that our fiducial MW-sized halo is not well represented by the formula of Bullock et al., which agree with the findings by Chen & Jing (2002).

These results already suggest that significant differences in the angular momentum distributions (AMDs) of halos with and without SI are not expected. To compute the AMD we find first, for each particle, the specific angular momentum component along \mathbf{J}_{vir} , calling it j . We then divide the sphere of radius R_{vir} in spherical shells and each of these shells is in turn divided in four quadrants. Differences in the number of particles between cells for most of them are below a factor of two. Only a small fraction of these cells have negative j values and we reject them in the further calculation of the AMD; notice, however, that these particles with negative j can have a significant effect on the angular momentum problem and the formation of bulges (van den Bosch et al. 2002). Cells are ranked according to their j value and $M(<j)$ profiles are then built by counting the cumulative mass in cells with angular momentum smaller than j . Figure 9 shows the $M(<j)$ profiles for halos $G1$ and $Cl1$ (panels a and b, respectively, where circles are for CDM and squares for $\sigma_{DM} = 0.5$). Mass and angular momentum are given in M_{vir} and j_{max} units, respectively, where j_{max} is the maximum value reached by j . We have also plotted in Figure 9 the analytical form of $M(<j)$ proposed by Bullock et al. (2001) with $\mu = 1.25$; the line intends to guide the eye, it is not a fit to our numerical results. The effect of the dynamical expansion of the core is seen only at low j . There is less mass, for a given j , in SI halos or, for the same fraction of mass, CDM halos have less rotational support. However, the difference between the CDM and the SI profiles is so small that SIDM can not account for the differences between the predicted angular momentum

distribution of the CDM model and that determined for dwarf galaxies (van den Bosch, Burkert, & Swaters 2001).

4. SUBHALO POPULATION

In previous works on SIDM it was suggested that the number of subhalos in MW-sized halos should be lower than that predicted in CDM because subhalos are supposed to form with a lower concentration and/or because, the hot environment of a SIDM halo evaporates its subhalos. What do we see in our simulations? For halos $G1_{3.0}$, $G2_{3.0}$, and $G3_{3.0}$ the evaporation effect is strong and most substructure is erased (see, for example, circles in Fig. 10, left panel). For $\sigma_{DM} = 0.5$ and $0.1 \text{ cm}^2 \text{ gr}^{-1}$ (halos $G1_{0.1}$ and $G1_{0.5}$), the effect is less pronounced but the number of subhalos is still less than in the CDM MW-sized halos, although at the low velocity end ($v_{\max} = 20 \text{ kms}^{-1}$), the number of subhalos becomes larger. A similar behavior is seen in the halo $G1_{0.5/V}$, where the effective σ_{DM} of the MW-sized halo is $\approx 0.2 \text{ cm}^2 \text{ gr}^{-1}$. The subhalo v_{\max} -function of the halo $G1_{1.0/V}$ lies slightly above of the CDM one. The v_{\max} -function of subhalos seems to be sensitive to the effective σ_{DM} of the host halo rather than that of the subhalos. In any case, halos $G1_{0.1}$, $G1_{0.5}$, $G1_{0.5/V}$, and $G1_{1.0/V}$ have *at least* as many subhalos with $v_{\max} \lesssim 25 \text{ kms}^{-1}$ as the CDM MW-sized halo. Thus, we can conclude that the *substructure problem* (Klypin et al. 1999; Moore et al. 1999) is not solved by a SIDM model with $\alpha \leq 1$ and reasonable values of σ_0 , at least at the low v_{\max} end of the velocity function.

The explanation of why the survival time of subhalos

in a SIDM scenario is comparable or even longer than the one in the collisionless CDM cosmology resides probably in the fact that the host halo tidal force, responsible for the disruption of substructure along with dynamical friction, in the center is not as strong as in the CDM case. There may also intervene a numerical effect: the cores of subhalos, where the action of the self-interaction is important, are not resolved in the simulations in such a way that subhalo density profiles are very similar to those of CDM ones. Notice, however, that this argument applies only to relatively small effective σ_{DM} values: if σ_{DM} is very high, subhalo concentrations can be modified significantly by particle evaporation.

For completeness we have also plotted the cumulative v_{\max} -function for the fiducial cluster-sized halo *C11* with the different values of (σ_0, α) (Fig. 10, right panel). The total number of subhalos within the SIDM cluster-sized halos (a sphere of $1.5 h^{-1}\text{Mpc}$ radius was used) is only slightly smaller than for the CDM halo, excepting the cases with $(\sigma_0, \alpha) = (3.0, 0.0)$ and $(0.5, 0.0)$. It is interesting to notice that the evaporation constraint on the Fundamental Plane of elliptical galaxies within the clusters set namely a maximum value of $\sigma_{DM} \approx 0.5 \text{ cm}^2\text{gr}^{-1}$ (when $\alpha = 0$) according to Gnedin & Ostriker (2001). Regarding the shape of the v_{\max} -function, in the range of 200-300 kms^{-1} , the SI cluster-sized halos have more subhalos than the corresponding CDM halo but the contrary happens at the low- v_{\max} end, SI cluster-sized halos have less subhalos than the CDM halo. This could be attributed to a longer survival time of massive subhalos. We do not expect a serious observational conflict related to the subhalo population in SIDM cluster-sized halos with $(\sigma_0, \alpha) = (0.1, 0.0)$, $(0.5, 1.0)$ and $(1.0, 1.0)$.

5. VIABILITY OF THE SIDM COSMOGONY

Spergel & Steinhard (2000) proposed the SIDM model in an attempt to overcome the apparent discrepancy between the cuspy halos predicted by CDM and the shallow halos inferred from observations of dwarf and LSB galaxies (Moore 1994; Flores & Primack 1994; Burkert 1995; de Blok & McGaugh 1997). This discrepancy has been challenged by Swaters, Madore, & Trewella (2000), van den Bosch, Robertson, Dalcanton, & de Blok (2000), and van den Bosch & Swaters (2001) who concluded that the spatial resolution of observed rotation curves was not sufficient to put constraints on cosmological models. However, more recent observational studies, using the highest sensitivity and spatial resolution in HI, H α and CO lines show that halos of dwarf and LSB galaxies are actually less concentrated in the center than the prediction of the CDM model (Côté, Carignan, & Freeman 2000; Blais-Ouellette, Amram, & Carignan 2001; Bolatto et al. 2002; Amram & Garrido 2002; de Blok et al. 2001a, 2001b; Marchesini et al. 2002). Also, there are pieces of evidence of soft cores in normal disk galaxies (e.g., Corsini et al. 1999; Borriello & Salucci 2001; Salucci 2001) and in elliptical galaxies (Keeton 2001), although the evidence is less direct than in the case of dwarf and LSB galaxies.

Assuming the non-singular isothermal or pseudo-isothermal halo models, several authors have tried to find scaling laws for halo cores. In a pioneering paper, Kormendy (1990) derived the halo component parameters of some dSph and spiral galaxies, and concluded that halos

with larger central velocity dispersions, σ , have larger core radii, r_c , and smaller central densities, ρ_c (see also Burkert 1995; Salucci & Burkert (2000)). The correlations they found have a large scatter. On the other hand, for normal spirals, the halo parameters depend strongly on the assumed stellar M/L ratios, and for dSph galaxies the observational uncertainties are large.

More recently, Firmani et al. (2000, 2001a), in an effort to infer the core halo scaling laws, have analyzed a sample of dwarf and LSB galaxies with high-quality rotation curves and cluster of galaxies studied with gravitational lensing. They used the non-singular isothermal model and took into account the effect of gravitational drag by the baryon matter on the halo for the LSB galaxies. Firmani et al. found that: (i) ρ_c exhibits a large scatter, while a correlation with the maximum circular velocity, v_{\max} (or σ), is not obvious, and (ii) r_c and v_{\max} tend to correlate with a slope smaller than 1. The different mass models of observational samples presented by several authors lead to a similar conclusion (Côté et al. 2000 for dIrr's; Verheijen 1997, and de Blok et al. 2001b for LSB galaxies). All these authors use different M/L ratio assumptions (not too important for dwarfs) and apply either the non-singular isothermal or the pseudo-isothermal models. For the former case, $\rho_{c,-1} = 0.54\rho_c$ and $r_{c,-1} = 0.7r_c$, while for the latter $\rho_{c,-1} = 0.5\rho_c$ and $r_{c,-1} = r_c$. We estimate $\rho_{c,-1}$ and $r_{c,-1}$ from the Firmani et al. compilation and the works mentioned above. From Verheijen (1997) and de Blok et al. (2001b) we use their fits with the equal M/L ratio, and for the Côté et al. (2000) data on nearby dwarfs we assume $h = 0.65$. In the range of the observations, $v_{\max} \sim 40 - 250 \text{ kms/s}$, $\rho_{c,-1}$ oscillate roughly between 10^{16} and $10^{17} h^2\text{M}_\odot\text{Mpc}^{-3}$ with the average at $\approx 3 \times 10^{16} h^2\text{M}_\odot\text{Mpc}^{-3}$. The radius $r_{c,-1}$ increases with v_{\max} but the scatter is very large; for $v_{\max}=100 \text{ kms}^{-1}$, $r_{c,-1} \approx 3h^{-1}\text{kpc}$ on average. Note that for the LSB galaxy data from Verheijen (1997) and de Blok et al. (2001b) the inferred central densities and core radii are upper and lower limits, respectively. The formation of a central disk contracts adiabatically the inner halo. For a typical LSB galaxy, the halo core radius could have shrunked by a factor of ~ 1.5 after disk formation (Firmani & Avila-Reese 2000; Firmani et al. 2001a), increasing the central density by a factor of ~ 2 . For higher surface brightness galaxies these factors are larger. Observations show that the fitted halo central density indeed increases with disk surface brightness (Verheijen 1997; Swaters 1999). Taking into account a correction for the further halo contraction, the scatter in the plot $\rho_{c,-1}-v_{\max}$ diminishes and the correlation between $r_{c,-1}$ and v_{\max} becomes tighter.

At the scale of cluster of galaxies, the highest resolution mass distribution analyses were done on the basis of either strong gravitational lensing studies or high-resolution X-ray studies of the intracluster medium. For the cluster CL0024+1654 studied with strong gravitational lensing techniques (Tyson, Kochanski, & dell'Antonio 1998), Firmani et al. (2001a) found a central density similar to those of their dwarf and LSB galaxy sample. From Firmani et al., we calculate $\rho_{c,-1} = 2.6 \times 10^{16} h^2\text{M}_\odot\text{Mpc}^{-3}$ and $r_{c,-1} = 45.5h^{-1}\text{kpc}$ ($v_{\max}=2400\text{kms}^{-1}$). Most of the measured cluster mass distributions from high-resolution X-ray studies of cluster of galaxies (mainly with the Chandra satellite) are well fitted by both the NFW profile

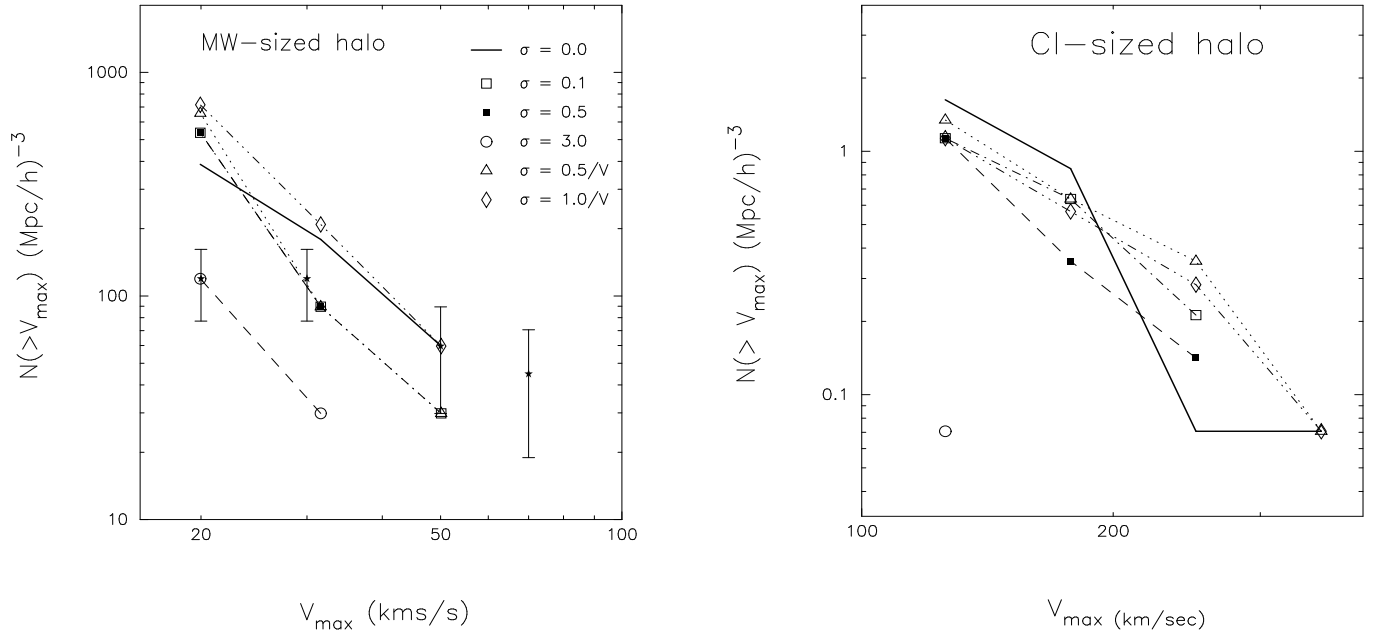


FIG. 10.— Cumulative v_{\max} -function of MW- (left panel) and cluster-sized halos (right panel). All $G1$ ($Cl1$) subhalos with v_{\max} greater than 20 kms^{-1} (126 kms^{-1}) and within a sphere of radius $200 h^{-1} \text{ kpc}$ ($1.5 h^{-1} \text{ Mpc}$) were counted. The averaged v_{\max} -function from satellites of MW and Andromeda is represented by stars (taken from KKVP99) and it is shown in left panel. Error bars are just Poisson errors. The number of subhalos in SI halos with a reasonable σ_{DM} (i.e., with a σ_{DM} that also satisfies other observational constrains) is comparable to the one seen in the CDM prediction. Notice that there is only one subhalo within halo $Cl1_{3.0}$ and in the last two v_{\max} bins of halo $Cl1_{0.0}$. The presence of few more massive subhalos in SI cluster-sized halos could be explained by a longer survival time of these halos with respect to the survival time of subhalos in the CDM halo.

and the pseudo-isothermal model. From the fitting parameters reported for the clusters A1835 (Schmidt, Allen, & Fabian 2001), A2390 (Allen, Ettori & Fabian 2001), RXJ1347.5-1145 (Allen, Schmidt, & Fabian (2001)), and EMSS 1358+62 45 (Arabadjis, Bautz & Garmire 2002; this cluster is at $z = 0.328$), we calculate $\rho_{c,-1} = 2.8 \times 10^{16}$, 2.0×10^{16} , 9.1×10^{16} and $\geq 2.4 \times 10^{17} h^2 \text{ M}_{\odot} \text{ Mpc}^{-3}$, $r_{c,-1} = 32.5$, 37.5 , 22.5 and $< 6 h^{-1} \text{ kpc}$, and $v_{\max} = 1843$, 1785 , 2290 and 1008 kms^{-1} , respectively. Note, however, that the inclusion of the adiabatic cluster halo contraction due to a cD or another central galaxy would favor more extended shallow cores.

The dotted lines in Figure 4 encompass roughly the 2σ dispersion of the observational inferences of $\rho_{c,-1}$ and $r_{c,-1}$ versus v_{\max} for the dwarf and LSB galaxies and the cluster of galaxies described above. The dashed lines are lines representative of the average behavior of the data. In Figure 4 were also plotted the model predictions for different values of σ_{DM} . At cluster scales the Λ CDM halos seem to be in agreement with observations. However, at galaxy scales they are roughly a factor of ten denser at the radius $r_{c,-1}$. Extrapolating to scales of dwarf galaxies this factor would be even larger. On the other hand, a SIDM model with an effective σ_{DM} as large as $3.0 \text{ cm}^2 \text{ gr}^{-1}$ produces halos with a large variety of inner structures. As discussed in §3, for these values of σ_{DM} the core collapse is triggered in a time scale smaller than the Hubble time. However, we also have seen that the core collapse could be delayed by late major mergers or even stopped by a continuous injection

of thermal energy from the hotter particles of the ambient in which the halo is embedded. Thus, in a cosmogony with a relatively high effective cross section, some halos could show shallow inner density profiles (e.g., elliptical and dwarf galaxy halos), while those which are isolated would be in the core collapse phase showing cuspy inner density profiles (e.g., LSB galaxy halos). Nevertheless, the major conflict in this case is that substructure is strongly erased; for example, for $\sigma_{DM} = 3 \text{ cm}^2 \text{ gr}^{-1}$, most subhalos in cluster- and galaxy-sized halos are evaporated, in complete disagreement with observations (Fig. 10).

The SIDM simulations with $(\sigma_0, \alpha) = (0.1, 0.0)$ and $(0.5, 0.0)$ show that at galaxy scales the central densities of the halos agree roughly with observations, the latter case producing probably slightly shallower halos than observed. However, at the cluster scales the halos in both cases are too shallow w.r.t. observations. We are then left with SIDM models in which σ_{DM} varies as the inverse of v_{12} . For the cases explored here, $(\sigma_0, \alpha) = (0.5, 1.0)$ and $(1.0, 1.0)$, halos at galaxy and cluster scales fall within the observational range, and ρ_c and the halo soft core fraction are approximately constant with scale (v_{\max}). Unfortunately, we can not explore the inner density profiles of the (sub) halos at the scales of dwarf galaxies because of they are resolved with too few particles. Extrapolating, it seems that halos at the scales of dwarf galaxies would remain as shallow as the larger ones. A weak hint that this could be happening comes from measuring the c_M concentration parameter for subhalos of MW-sized halos. This parame-

ter characterizes the shape of the density profiles at radii $\sim 0.03 - 0.1R_{vir}$. In the central panels of Figure 7 one sees that c_M for subhalos of halos $G1_{0.5/V}$, $G2_{0.5/V}$, and $G1_{1.0/V}$ is on average lower than that corresponding to CDM subhalos. To a first approximation, we expect ρ_c to be independent of v_{max} when $\sigma_{DM} \propto 1/v_{12}$ because N_{col} (eq. 4) or the collisional probability P do not depend in this case on v_{12} . However, N_{col} or P also depend on the local density and this is typically larger for smaller halos.

The satellite cumulative v_{max} -function of the halo $G1$ with $(\sigma_0, \alpha) = (0.5, 1.0)$ is slightly higher than the one of the corresponding CDM halo at the low velocity limit, and then drops by a big factor, giving good agreement with observations for $v_{max} \gtrsim 30 \text{ km s}^{-1}$ (Fig. 10). For the $(\sigma_0, \alpha) = (1.0, 1.0)$ case, the function lies above of the CDM prediction up to $v_{max} = 50 \text{ km s}^{-1}$. As explained in §4, this could be due to the softer inner gravitational potential of the SIDM halos with respect to the CDM ones. For the explored range of the SI parameter space, it seems that the main influence on the number and structure of subhalos comes from the scattering properties of the host halo rather than those intrinsic to subhalos (collisions only between subhalo particles). In §3.2 we have seen indeed how structures of subhalos with similar σ_{DM} differ because the effective σ_{DM} of the host halos are different.

In conclusion, among the SIDM models studied in this paper, those with σ_{DM} inversely proportional to v_{12} are able to produce halo cores shallower than CDM and with central densities roughly constant with v_{max} . However, the substructure problem for MW-sized halos is not solved. Reionization has been proposed as a mechanism able to inhibit the formation of dwarf galaxies within the large population of predicted small CDM halos (Bullock et al. 2000), in such a way that the substructure excess would not be longer a critical issue. Nevertheless, a potential problem with the Tully-Fisher relation of dwarf galaxies would remain (Avila-Reese et al. 2001).

Recently, HO carefully analyzed several observational constraints for the SIDM model. Their study is mostly based on analytical estimates calibrated on basis of previous numerical results. These estimates agree with the results obtained here for SIDM models with a constant σ_{DM} and with a σ_{DM} inversely proportional to v_{12} . If we add the constrain given by the satellite overabundance in MW-sized halos, then the region of allowed (σ_0, α) values becomes smaller than in HO since models with $\alpha \lesssim 1$ also would be ruled out. However, as mentioned above, this constrain is weaker than the others because the satellite excess problem could be solved invoking reionization.

HO have introduced one extra constrain, namely the formation of supermassive black holes (SMBH) due to SI (Ostriker 2000). According to their estimates and using the observed mass of the central SMBH of our Galaxy and the lack of a SMBH in the bulge-less galaxy M33, they conclude that σ_{DM} should be smaller than $0.02 \text{ cm}^2 \text{ gr}^{-1}$ for any value of $\alpha \leq 1$. A critical assumption of this constrain is that the dark halo initially has the typical cuspy CDM density profile, i.e., the establishment of the soft core by SI occurs only at time scales close to a Hubble time. In fact, the mass of the SMBH formed by accretion of SIDM is extremely sensitive to the inner halo density profile slope. For a slope shallower than -1 this mass is

much less than $10^3 M_\odot$ for $\alpha \leq 1$ (see Fig. 1 in HO). Our simulations show that the evolving time scales under SI for the cases analyzed here are much less than a Hubble time. The core expansion phase actually occurs in time scales close to the halo dynamical time (Figs. 1 and 5) for $\sigma_{DM} \sim 1 \text{ cm}^2 \text{ gr}^{-1}$. The calculations of halo evolution under SI of Firmani et al. (2001b) also show that the inner halo density profile flattens quickly, as the halo grows and virializes. So, accretion of SIDM could not be the relevant mechanism for the formation of SMBH and, therefore, the strong constraint of HO might not be valid. For the formation of SMBH other alternative mechanisms have been proposed (e.g., Granato et al. 2001).

6. CONCLUSIONS

A set of high-resolution N-body simulations has been run to study the structure and substructure of cluster- and MW-sized halos in a SI Λ CDM cosmology with cross sections $\sigma_{DM} = \sigma_0 (1/v_{100})^\alpha$, where σ_0 is in units of $\text{cm}^2 \text{ gr}^{-1}$, and v_{100} is the relative velocity in units of 100 km s^{-1} . Our main conclusions follows:

- For low values of σ_{DM} , when $N_{col} \lesssim 2-5$ at $z = 0$, and for a given mass, the lower the σ_{DM} , the smaller the core radii and the higher the central densities. This behavior may be reversed for high values of σ_{DM} . In this last case, the evolution of halos under SI is fast and the core collapse phase could begin well before $z = 0$. We analysed 2 cluster- and 3 MW-sized halos with $(\sigma_0, \alpha) = (3.0, 0.0)$ and different mass assembly histories. We have found that they go through the core collapse phase, although this phase can be delayed significantly for some halos by both dynamical heating due to *major mergers* (but not smooth mass accretion) and the evaporation of (sub)halo particles interacting with the hot particles of the host halo.

- The SIDM halos expand their cores due to a heat inflow from the hotter surroundings. Since the core heat capacity, C , is positive, this process leads to the isothermalization of the core. After the core maximum expansion, C becomes negative down to smaller radii. Then the gravothermal instability triggers and the core collapses. The system moves from a minimum to a maximum entropy state. If the halo periphery is heated and the temperature becomes higher than in the core, the heat inflows to the core and the core expands until the overall halo isothermalizes. This process delays the core collapse, but will hardly reverse the gravothermal instability to a runaway core expansion.

- Present day halos with $N_{col} \lesssim 2-5$ are still expanding their cores or have just had the gravothermal catastrophe triggered. The inner density profiles when isolated (host) are flattened by SI only in the innermost regions, $r < 0.05R_{vir}$. When σ_{DM} is constant, massive halos are supposed to be the most affected by SI ($N_{col} \propto \rho v_{max}$). For typical cluster-sized halos to have $N_{col} \lesssim 2-5$, σ_{DM} should be smaller than $\approx 0.5 \text{ cm}^2 \text{ gr}^{-1}$. For $\sigma_{DM} \lesssim 0.5 \text{ cm}^2 \text{ gr}^{-1}$, the lower the v_{max} , the higher the ρ_c . On the other hand, when $\sigma_{DM} \propto 1/v_{12}$, this trend is much weaker: ρ_c remains almost constant with v_{max} . We compare the predicted core densities and radii as well as the scaling laws of the halo cores with those inferred from the observations of dwarf and LSB galaxies and cluster of galaxies. The SIDM models with $\sigma_{DM} = 0.5 - 1.0 (1/v_{100}) \text{ cm}^2 \text{ gr}^{-1}$ are favored. With these values of σ_{DM} , N_{col} is smaller than

2-5 from galaxy- to cluster-sized halos.

-We find that the structure and population of subhalos are determined by the interaction between the hot host halo particles and the cooler subhalo particles rather than by internal processes in the subhalos. Our simulations show that overall SIDM subhalos become puffier than their CDM counterparts and that they are completely evaporated in the limit of high σ_{DM} . For all the (σ_0, α) values used here, we do not see signs of a core collapse in subhalos, but we warn that this result can be masked by the poor mass resolution of the simulations at the subhalos scales.

-The number of subhalos within MW-sized halos is largely suppressed for $(\sigma_0, \alpha) = (3.0, 0.0)$. The cumulative v_{\max} -functions of models $(\sigma_0, \alpha) = (0.1, 0.0)$, $(0.5, 0.0)$ and $(0.5, 1.0)$ agree roughly with the observations for $v_{\max} \gtrsim 30 \text{ km s}^{-1}$, but at the low v_{\max} end they lie slightly above the corresponding CDM one. For $(\sigma_0, \alpha) = (1.0, 1.0)$, this function is higher than the CDM at all v_{\max} . Subhalos may survive a longer time in SIDM halos than in CDM ones because the inner tidal force in the former is weaker than in the latter. Our results show that the range of (σ_0, α) values in which the SIDM scenario is interesting does not solve the potential problem of the excess of substructure in MW-sized halos.

- The SIDM halos have more angular momentum at a given mass shell than their CDM counterparts. However, this extra angular momentum is small and does not solve the conflict between the measured angular momentum distribution in CDM halos and that inferred from observations for dwarf galaxies. On the other hand, the SIDM core ha-

los are indeed rounder than their CDM counterparts, but they are not spherical. This roundness is not only seen in the core, it can extend all the way to the virial radius of the halo.

We conclude that the problem of cuspy halos in the Λ CDM cosmology may be solved by introducing a modest dark matter cross section inversely proportional to the relative velocity of interaction, $\sigma_{DM} \approx 0.5 - 1.0(1/v_{100}) \text{ cm}^2 \text{ gr}^{-1}$. On the other hand, our simulations show that for these values of σ_{DM} , the number of subhalos in MW-sized halos is close to that of the CDM counterparts. Our simulations also show that SI flattens the inner density profiles of growing CDM halos since early epochs in such a way that the grow of super massive black holes by accretion of SIDM is not an efficient process. A remaining interesting question is whether the CDM candidate particles may be predicted with the cross sections after their decoupling preferred by our results.

We are grateful to Anatoly Klypin and Andrey Kravtsov for kindly providing us a copy of the ART code in its version of multiple mass, and for our enlightening discussions. The authors thank also the anonymous referee for constructive suggestions. P.C. would like to thank A. Watson and W. Henney for the use of a PC in which part of the ART simulations were done. Part of the ART simulations were also performed at the Dirección General de Servicios de Cómputo Académico, UNAM, using an Origin-2000 computer. This work was supported by CONACyT grants 33776-E to V.A. and 36584-E to P.C.

REFERENCES

- Allen, S.W., Ettori, S. & Fabian, A.C. 2001, MNRAS, 324, 877
 Allen, S. W., Schmidt, R. W., & Fabian, A. C. 2001, MNRAS, 328, L37
 Amram, P., Garrido, O. 2002, in "Galaxies: the third dimension", Eds. M. Rosado, L. Binette, & L. Arias, ASP Conf. Series, in press (astro-ph/0202475)
 Arabadjis, J.S., Bautz, M.W. & Garmire, G.P. 2001, ApJ, 572, in press
 Avila-Reese, V., Firmani, C. & Hernández, X. 1998, ApJ, 505, 37
 Avila-Reese, V., Firmani, C., Klypin, A. & Kravtsov, A.V. 1999, MNRAS, 310, 527
 Avila-Reese, V., Colín, P., Valenzuela, O., D'Onghia, E., & Firmani, C. 2001, ApJ, 559, 516
 Balberg, S., Shapiro, S.L., & Inagaki, S. 2002, ApJ, 568, 475
 Binney, J., & Tremaine, S. 1987, "Galactic Dynamics", Princeton UP
 Blais-Ouellette, S., Amram, P., & Carignan, C. 2001, AJ, 121, 1952
 Bolatto, A. D., Simon, J. D., Leroy, A., Blitz, L. 2002, ApJ, 565, 238
 Borriello, A., Salucci, P. 2001, MNRAS, 323, 285
 Bullock, J.S., Dekel, A., Kolatt, T.S., Kravtsov, A.V., Klypin, A.A., Porciani, C., & Primack, J.R. 2001, ApJ, 555, 240
 Burkert, A. 1995, ApJ, 477, L25
 Burkert, A. 2000, ApJ, 534, L143
 Chen, D.N., & Jing, Y.P. 2002, MNRAS, submitted (astro-ph/0201520)
 Corsini, E. M. et al. 1999, A&A, 342, 671
 Côté, S., Carignan, C., & Freeman, K. C. 2000, AJ, 120, 3027.
 Davé, R., Spergel, D.N., Steinhardt, P.J., & Wandelt, B.J. 2001, ApJ, 547, 574
 de Blok W.J.G., & McGaugh S.S., 1997, MNRAS, 290, 533
 de Blok, W. J. G., McGaugh, S. S., Bosma, A., & Rubin, V. C. 2001a, ApJ, 552, L23
 de Blok, W. J. G., McGaugh, S. S., & Rubin, V. C. 2001b, AJ, 122, 2396
 Firmani, C. & Avila-Reese, V. 2000, MNRAS, 315, 457
 Firmani, C., D'Onghia, E., Avila-Reese, V., Chincarini, G., & Hernández, X. 2000, MNRAS, 315, L29
 Firmani, C., D'Onghia, E., Chincarini, G., Hernández, X., & Avila-Reese, V. 2001a, MNRAS, 321, 713
 Firmani, C., D'Onghia, E., & Chincarini, G. 2001b, MNRAS submitted (astro-ph/0010497)
 Flores, R., & Primack, J.R. 1994, ApJ, 427, L1
 Franx, M., Illingworth, G., & de Zeeuw, T. 1990, ApJ, 383, 112
 Granato, G. L., Silva, L., Monaco, P., Panuzzo, P., Salucci, P., De Zotti, G., Danese, L. 2001, MNRAS, 324, 757
 Gibbs, W. R., 1994, Computation in Modern Physics, World Scientific Publishing
 Gnedin, O.Y., & Ostriker, J.P. 2001, ApJ, 561, 61
 Hennawi, J.F., & Ostriker, J.P. 2001, ApJ submitted (astro-ph/0108203) (HO)
 Hockney, R.W., & Eastwood, J.W. 1981, Computer Simulations Using Particles (New York: McGraw-Hill)
 Kauffmann, G., White, S. D. M., & Guideroni, B. 1993, MNRAS, 264, 201
 Keeton, C. R. 2001, ApJ, 561, 46
 Klypin, A.A., Gottlober, S., Kravtsov, A.V., Khokhlov, A.M. 1999, ApJ, 516, 530
 Klypin, A.A., Kravtsov, A.V., Bullock, J.S., & Primack, J.R. 2001, ApJ, 554, 903
 Klypin, A.A., Kravtsov, A.V., Valenzuela, O., Prada, F. 1999, ApJ, 522, 82
 Kochanek, C.S., & White, M. 2000, ApJ, 543, 514 (KW)
 Kormendy, J. 1990, in "Evolution of the Universe of Galaxies", Ed. R.G. Kron, ASP Conf. Ser. 10, p.33
 Kravtsov, A.V., Klypin, A.A., & Khokhlov, A.M. 1997, ApJS 111, 73
 Lokas, E.L., Mamon, G. A. 2001, MNRAS, 321, 155
 Lynden-Bell, D., & Wood, R. 1968, MNRAS, 138, 495
 Marchesini, D., D'Onghia, E., Chincarini, G., Firmani, C., Conconi, P., Molinari, E., Zacchei 2002, ApJ, in press (astro-ph/0202075)
 Meneghetti, M., Yoshida, N., Bartelmann, M., Moscardini, L., Springel, V., Tormen, G., White, S.D.M. 2001, MNRAS, 325, 435
 Miralda-Escudé, J. 2002, 564, 60
 Moore, B. 1994, Nature, 370, 629
 Moore, B., Ghigna, S., Governato, F., Lake, G., Quinn, T., Stadel, J., & Tozzi, P. 1999, ApJ, 524, L19
 Moore, B., Gelato, S., Jenkins, A., Pearce, F.R., & Quilis, V. 2000, ApJ, 535, L21
 Ostriker, J.P. 2000, Phys. Rev. Lett., 84, 23

- Quinlan, G.D. 1996, *NewA*, 1, 255
Salucci, P. & Burkert, A. 2000, *ApJ*, 537, L9
Salucci, P. 2001, *MNRAS*, 320, L1
Schmidt, R. W., Allen, S. W., & Fabian, A. C. 2001, *MNRAS*, 327, 1057
Spergel, D.N. & Steinhardt, P.J. 2000, *Phys. Rev. Lett.*, 84, 3760
Swaters, R. A. 1999, Ph.D. Thesis, Univ. of Groningen
Swaters, R.A., Madore, B.F., & Trewhella, M. 2000, *ApJ* in press (astro-ph/0001277)
Tyson, J. A., Kochanski, G. P., & dell'Antonio, I. P. 1998, *ApJ*, 498, L107
van den Bosch, F. C., Robertson, B. E., Dalcanton, J. J., & de Blok, W. J. G. 2000, *AJ*, 119, 1579.
van den Bosch, F.C., Burkert, A., & Swaters, R.A. 2001, *MNRAS*, submitted, (astro-ph/0105082)
van den Bosch, F.C., Abel, T., Croft, R.A.C., Hernquist, L., & White, S.D.M. 2002, *ApJ* submitted (astro-ph/0201095)
Verheijen, M. A. W. 1997, Ph.D. Thesis, Univ. of Groningen
Wandelt, B.D., Davé, R., Farrar, G.R., McGuire, P.C., Spergel, D.N., Steinhardt, P.J. (astro-ph/0006344)
Wechsler, R.H., Bullock, J.S., Primack, J.R., Kravtsov, A.V., & Dekel, A. 2001, *ApJ*, submitted, (astro-ph/0108151)
Yoshida, N., Springel, V., & White, S.D.M. 2000, *ApJ*, 535, L103
Yoshida, N., Springel, V., White, S.D.M., & Tormen, G. 2000, *ApJ*, 544, L87
Zhao, D.H., Mo, H.J., Jing, Y.P., & Börner, G. *MNRAS*, submitted (astro-ph/0204108)